9-2004

Extratropical Transition of Southwest Pacific Tropical Cyclones. Part II: Midlatitude Circulation Characteristics

Mark R. Sinclair
Embry-Riddle Aeronautical University, sinclam@erau.edu

Extratropical Transition of Southwest Pacific Tropical Cyclones. Part II: Midlatitude Circulation Characteristics

MARK R. SINCLAIR

Embry–Riddle Aeronautical University, Prescott, Arizona

(Manuscript received 23 April 2003, in final form 15 March 2004)

ABSTRACT

This second of two papers on extratropical transition (ET) over the southwest Pacific Ocean focuses on the variability of ET. A climatology of ET onset based on a previously described objective technique shows that ET commences 15° of latitude nearer the equator on average than similar cases from the Northern Hemisphere. Characteristic midlatitude circulation patterns accompanying ET near 30°S are identified by means of empirical orthogonal function (EOF) analysis of 50 storms. The first eigenvector pattern, explaining nearly half the circulation variability, expresses relaxed and enhanced pressure gradients south of the storm that define composites similar to ''cradled'' and ''captured'' classifications previously described for the southeast Indian Ocean. The second EOF distinguishes redeveloping from weakening storms. Reintensifying storms were located beneath strong cyclonic vorticity advection (CVA) near the equatorward entrance region of an upper jet whereas the upper jet was well to the west of weakening storms.

A survey of factors responsible for modulating central sea level pressure change during ET was conducted for the 50 storms. The quantity most strongly correlated with surface development was found to be CVA at the jet level. Extratropical reintensification occurred when the surface cyclone was located beneath the equatorward entrance region of an upper jet for storms between 28° and 34°S, and beneath the poleward exit jet region for storms farther south. Strongest examples of redevelopment each occurred beneath a potent double jet signature aloft, with maximum storm-relative upper-level CVA located directly above the surface low and net vorticity fluxes reflecting amplification of the upper wave. Weakening storms featured a weakening upper trough directly above the storm, with CVA to the east.

1. Introduction

This is the second of two papers on extratropical transition (ET) in the southwest Pacific Ocean basin. In the first (Sinclair 2002), a 28-yr climatology was constructed for TCs moving into middle latitudes. That study identified the average structure changes during ET in the southwest Pacific Ocean basin by compositing storms at various stages of ET. It showed that, on average, southwest Pacific tropical cyclones (TCs) start to encounter the baroclinic westerlies at around 20°S, resulting in increasing eastward and poleward motion and an early onset of extratropical transformation compared with their Northern Hemisphere (NH) counterparts. By 25°–30°S, virtually all southwest Pacific TCs undergoing ET have acquired characteristics of midlatitude storms, including asymmetric thermal and vertical motion fields, upper jet streaks, cold and warm frontogenesis regions, and a westward tilt with height.

This second companion paper addresses the issue of ET variability. Using data from 50 TCs that progress south of 35°S, the study will first identify the location of ET onset using an objective measure of thickness asymmetry similar to that proposed by Evans and Hart (2003, hereafter EH). This analysis will determine for the first time, the range of latitudes at which southwest Pacific TCs commence the process of ET. Second, this study will identify characteristic synoptic-scale signatures that accompany ET near 30°S. Storms that cross this latitude are entering New Zealand waters and forecasters there need to be alert to changes in track, intensity, and structure. Identifying characteristic patterns and how storms in each class evolve as they pass this latitude will help New Zealand forecasters anticipate the result as a storm enters New Zealand waters and recognize signatures that lead to severe events. At this latitude, the contribution from the environmental westerlies is increasing, resulting in acceleration and recurvature to the southeast. While most TCs are weakening at this latitude, a few reintensify as vigorous extratropical systems as a result of interaction with an active trough in the westerlies (Sinclair 1993b; Hill 1970). The potential for rapid track and intensity changes near this latitude compounds the difficulty associated with pre-

Corresponding author address: Dr. Mark R. Sinclair, Embry–Riddle Aeronautical University, 3700 Willow Creek Road, Prescott, AZ 86301.
E-mail: Mark.Sinclair@erau.edu

dicting the severity and duration of heavy precipitation, damaging winds, and wave events.

Simple composites such as those in Sinclair (2002) mask case-to-case variability and do not address the range of synoptic configurations between a TC and a midlatitude trough. There is much observational and theoretical evidence that there are distinct synoptic-scale flow patterns that lead to fundamentally different modes of midlatitude cyclone evolution (Davies et al. 1991; Thorncroft et al. 1993; Schultz et al. 1998; Sinclair and Revell 2000). Likewise, there is growing evidence that the changes in TC structure, motion, and intensity that occur during ET are highly dependent on the nature of the midlatitude circulation into which the TC moves. Harr and Elsberry (2000) attributed differences in the extratropical evolution of two North Pacific TC remnants to the different midlatitude circulation characteristics into which each TC moved. They proposed that the structure of the midlatitude environment was the primary factor that determined the rate of any reintensification of the TC remnant. Thorncroft and Jones (2000) and Browning et al. (1998) found that North Atlantic ET characteristics differ for storms interacting with cyclonic versus anticyclonic sheared waves. According to Thorncroft et al. (1993), cyclonically sheared waves are characterized by cyclonic wrap-up of the upper-level potential vorticity (PV) and a broad, deep surface cyclone while anticyclonically sheared waves lead to meridionally elongated upper-level PV anomalies and the development of cutoff lows. McTaggart-Cowan et al. (2001) found that the reintensification of Hurricane Earl was largely dependent on the midlatitude environment, with the nature of the hurricane remnants having comparatively little impact. Simulations by Ritchie and Elsberry (2003) confirmed the hypothesis that the intensity of extratropical redevelopment of an ex-TC depends strongly on the characteristics of the midlatitude circulation into which the TC is moving, but noted that favorable phasing of the TC with the approaching midlatitude trough can result in substantial enhancement of upper-level divergence, even for weaker midlatitude troughs.

Extratropical transition is sensitive to the geometry of the interaction between the decaying TC and the midlatitude environment into which the TC is moving. Harr et al. (2000) used empirical orthogonal function (EOF) analysis to identify two characteristic circulation patterns over the western North Pacific during ET. One pattern, in which ET occurred downstream from a large-amplitude midlatitude upper trough located northwest of the TC was called the *northwest pattern*, while the other pattern featured the TC embedded in a more zonal confluent flow about a large circulation center northeast of the TC (*northeast pattern*). Klein et al. (2000) compared storm evolution for these two environments. Storms moving into the northwest pattern tended to intensify more rapidly and take a meridional track while storms in the northeast pattern intensified only slowly and moved in a more zonal direction. Furthermore, the position of the primary midlatitude circulation relative to the poleward-moving TC was found to influence frontogenesis and energy transformations during ET. Sometimes, a trough interaction can invigorate the TC without ET occurring. Hanley (1999) and Hanley et al. (2001) found that the midlatitude PV anomalies that lead to ET in the North Atlantic are much deeper and wider than cases (Hanley et al. 2001) where a trough interaction results in strengthening of the hurricane without ET. However, when a broader midlatitude PV maximum associated with an approaching midlatitude trough interacted with the TC, a favorable upper-divergence environment for surface development was created near the equatorward entrance region of a downstream jet as the upper-level PV approached to within 1000 km of the TC.

These NH studies show that the nature and geometry of the midlatitude circulation plays a crucial (and probably the dominant) role in determining how the track, structure, and intensity of TCs change during ET. This study follows Harr et al. (2000) and Klein et al. (2000) in using EOF analysis to identify the more persistent midlatitude synoptic-scale signatures associated with ET in the southwest Pacific basin. While the basic idea of identifying different classes of storm evolution is similar to that of Sinclair and Revell (2000), we here use the objective tool of EOF analysis. The goal is to identify the range of different midlatitude circulation patterns that accompany ET and determine the impact of each on intensity, structure, and motion changes. Data limitations and resolution here preclude individual case analysis as detailed as previous NH studies. In particular, vertical resolution is insufficient to realistically depict potential vorticity anomalies or tropopause undulations, as in previous NH case studies (Browning et al. 2000; Thorncroft and Jones 2000). Instead, we identify the variety of distinct recurring larger-scale synoptic patterns that accompany ET from a large number of analyzed storms. One practical motivation for identifying synoptic patterns is the potential to improve forecasts of gross features of future storm evolution from the nature of the midlatitude flow into which the TC is moving.

The third part of this study will identify characteristic midlatitude synoptic patterns that accompany extratropical reintensification. Klein et al. (2000) described the ET process as having two stages. In the first stage (transformation), the TC undergoes structure changes as it interacts with the baroclinic westerlies, resulting in the appearance of asymmetric thermal and ascent fields characteristic of baroclinic midlatitude cyclones. However, Klein et al. (2000) describe a possible second stage (reintensification) that occurs when the transformed TC undergoes reintensification, usually in response to increasing upper-level cyclonic vorticity advection ahead of an approaching midlatitude trough. Memorable NH examples include the regeneration of Hurricane Hazel

as a powerful extratropical storm (Palmén 1958) and Hurricane Agnes, which produced one of the worst natural flooding disasters in United States history (Carr and Bosart 1978; DiMego and Bosart 1982a,b). Examples of reintensifying storms in the southwest Pacific basin include the *Wahine* storm that produced winds gusting to 75 m s^{-1} in New Zealand's capital city of Wellington (Hill 1970) and Cyclone Bola, which dropped more than 900 mm of rain over northern New Zealand (NZ) in March 1988 (Sinclair 1993b). While maximum winds in these storms are typically weaker than in the parent hurricane, the areas of damaging wind and heavy rain are typically much larger (Hart and Evans 2001), increasing the potential for loss of life and property.

It is hypothesized here that a period of coupling with the divergence quadrant of an upper jet is a necessary condition for extratropical redevelopment of the tropical cyclone. Sinclair (1993b) identified the arrival of an upper jet from the west as a trigger for extratropical reintensification of Cyclone Bola (March 1988), which occurred beneath a highly divergent double upper-jet configuration. The regeneration of Cyclone Patsy (December 1986) coincided with a period of coupling with the equatorward entrance region of an upper jet that remained ''phase locked'' with the poleward-moving storm (Sinclair 1993a). Foley and Hanstrum (1994) showed that the reintensification of Cyclone Herbie near western Australia coincided with a strengthening thickness gradient caused by the approach of a cold front and favorable coupling with the equatorward entrance region of an upper jet. Bosart and Lackmann (1995) showed that Tropical Storm David reintensified over the eastern United States in response to warming and upper ridging downstream of a rather weak midlatitude disturbance. This warming, caused by strong latent heat release and warm advection, strengthened the vorticity gradient above the storm. At this time, David was located beneath the equatorward entrance region of an upper-wind maximum. The remnant of David was extremely responsive to the weak forcing ahead of the weak upper trough because of near-neutral moist stability that favored vigorous ascent and preexisting low-level ''seed'' vorticity that had a large development response to the increased ascent. Harr and Elsberry (2000) emphasize the importance of rotational frontogenesis in reinforcing the dynamical support for coupling with the approaching midlatitude trough. Although not directly implicated in that study, a downstream jet and strengthening downstream ridge again were accessory factors.

Following a brief description of available data (section 2), the location of ET onset is identified from an objective method. This is used to construct a climatology of ET onset and identify the typical synoptic setting accompanying ET onset (section 3). Section 4 identifies several characteristic synoptic signatures as the TC passes 30°S and describes the evolution within each class. In section 5, we identify the synoptic configurations that favor TC reintensification and diagnose the processes responsible. Section 6 comprises a summary and concluding remarks.

2. Data and methodology

a. Data sources

As outlined in Sinclair (2002), tropical cyclone best track and intensity data for the southwest Pacific basin are based on an archive developed by the New Zealand Meteorological Service (NZMS), henceforth referred to as the NZMS archive. The database compiles time, location, and estimated intensity, plus text comments, for all detected storms since 1939. Storms are tracked until their demise, including any extratropical phase. In this ocean basin, observational data prior to the advent of satellites are sparse, resulting in many TCs going undetected. Accordingly, only storms from 1970 onward are incorporated in this study. Unfortunately, the NZMS archive does not usually record the time of ET. An examination of Joint Typhoon Warning Center (JTWC) archives finds that they also did not record the time of ET. In this study, the objective method of EH is adapted to identify the time of ET onset (section 3).

Sinclair (2002) showed that southwest Pacific TCs that made it as far south as 35°S had completed ET and transformed to baroclinic extratropical cyclones. Here, we again identify a set of cyclones completing ET as those TCs that are tracked poleward of 35°S in the NZMS archive. In the period 1970–97, 81 TCs were tracked poleward of 35°S. Twenty-nine of these that spent their life east of 170°W were not included because of the lack of observational data over that region. The remaining 50 storms between Australia and 170°W during 1970–97 formed the TC population for this study. Table 1 is a summary of these storms.

Gridded reanalysis datasets from the National Centers for Environmental Prediction (NCEP) are utilized here for synoptic and diagnostic analysis. These comprise twice-daily analyses of geopotential height, wind, temperature, relative humidity, and vertical P velocity from the NCEP–NCAR reanalysis dataset (Kalnay et al. 1996) on a 2.5° × 2.5° latitude–longitude grid. As discussed in Sinclair (2002), the study region lies downwind from several rawinsonde and surface synoptic observation (SYNOP) stations near Australia and NZ, with additional island stations north of 30°S. In more recent years, a wide variety of satellite-derived products have also been assimilated into the analysis. Data coverage and analysis resolution are clearly not adequate to depict the hurricane's tight inner core, nor are they able to diagnose mesoscale details of ET to the extent that the NH studies referenced earlier have. Despite these limitations, Sinclair (2002, 1993a,b) showed that the 2.5°-resolution analyses are able to at least portray synoptic-scale influences on the structure, motion, and intensity of TCs in this region.

TABLE 1. List of southwest Pacific tropical cyclones during 1970–97 progressing poleward of 35°S.

Name	Start date	Start location	End date	End location
Rosie	30 Dec 1970	14.7°S, 164.0°E	4 Jan 1971	40.6°S, 169.1°E
Lena	14 Mar 1971	15.1°S, 157.5°E	23 Mar 1971	39.1°S, 159.3°W
Althea	21 Dec 1971	14.0°S, 157.3°E	30 Dec 1971	38.6°S, 166.0°E
Yolande	17 Mar 1972	15.2°S, 177.5°E	23 Mar 1972	36.3°S, 161.0°E
Kirsty	25 Feb 1973	13.6°S, 157.4°E	1 Mar 1973	39.0°S, 160.0°E
Nessie	19 Jan 1974	20.0°S, 162.2°E	22 Jan 1974	37.3°S, 177.2°E
Pam	30 Jan 1974	15.0°S, 177.8°W	7 Feb 1974	37.5°S, 161.0°E
Zoe	5 Mar 1974	18.9°S, 151.7°E	18 Mar 1974	38.2°S, 178.9°W
Alice	20 Mar 1974	17.2°S, 149.1°E	30 Mar 1974	40.7°S, 160.0°E
Val	29 Jan 1975	13.8°S, 176.5°W	5 Feb 1975	37.5°S, 171.0°W
Alison	4 Mar 1975	16.2°S, 172.5°E	11 Mar 1975	36.0°S, 171.2°E
Elsa	21 Jan 1976	14.2°S, 167.5°E	26 Jan 1976	35.0°S, 170.0°E
Colin	26 Feb 1976	10.0°S, 154.0°E	7 Mar 1976	46.0°S, 157.0°E
Jan	16 Apr 1976	14.8°S, 162.0°E	21 Apr 1976	40.0°S, 176.5°W
Watorea	25 Apr 1976	9.0°S, 153.8°E	30 Apr 1976	38.0°S, 177.7°W
Norman	9 Mar 1977	12.0°S, 168.0°E	24 Mar 1977	40.0°S, 177.0°W
Hal	7 Apr 1978	13.0°S, 145.0°E	22 Apr 1978	41.3°S, 179.0°W
Fay	27 Dec 1978	10.0°S, 175.0°E	31 Dec 1978	36.0°S, 174.0°W
Henry	29 Jan 1979	13.6°S, 167.6°E	5 Feb 1979	46.0°S, 175.0°E
Paul	7 Jan 1980	21.5°S, 149.0°E	12 Jan 1980	47.0°S, 161.0°E
Sina	10 Mar 1980	15.5°S, 159.0°E	16 Mar 1980	50.0°S, 173.0°W
Freda	26 Feb 1981	15.5°S, 144.6°E	9 Mar 1981	35.0°S, 169.8°E
Gyan	18 Dec 1981	9.0°S, 172.0°E	29 Dec 1981	41.0°S, 166.3°E
Hettie	24 Jan 1982	18.2°S, 166.1°E	6 Feb 1982	40.0°S, 156.0°W
Bernie	1 Apr 1982	5.0°S, 158.3°E	14 Apr 1982	40.0°S, 167.5°W
Monica	25 Dec 1984	12.8°S, 147.0°E	2 Jan 1985	50.0°S, 167.0°E
Hina	11 Mar 1985	16.5°S, 174.7°E	20 Mar 1985	38.0°S, 155.0°W
Patsy	13 Dec 1986	10.4°S, 172.7°E	22 Dec 1986	44.5°S, 177.7°E
Bola	24 Feb 1988	12.0°S, 180.0°E	11 Mar 1988	41.8°S, 170.8°E
Dovi	8 Apr 1988	15.0°S, 170.9°E	18 Apr 1988	44.3°S, 162.6°W
Eseta	17 Dec 1988	14.3°S, 166.3°E	28 Dec 1988	36.3°S, 170.5°E
Delilah	30 Dec 1988	17.3°S, 150.1°E	7 Jan 1989	37.1°S, 168.3°E
Harry	8 Feb 1989	17.2°S, 160.9°E	23 Feb 1989	49.0°S, 175.9°E
Nancy	28 Jan 1990	18.0°S, 156.0°E	8 Feb 1990	40.0°S, 170.9°E
Daman	15 Feb 1992	12.6°S, 170.0°E	23 Feb 1992	51.0°S, 158.0°W
Esau	25 Feb 1992	15.4°S, 168.5°E	9 Mar 1992	37.5°S, 179.0°W
Fran	5 Mar 1992	13.0°S, 174.7°W	21 Mar 1992	35.5°S, 166.0°W
Mick	5 Feb 1993	16.5°S, 173.0°W	11 Feb 1993	36.0°S, 179.0°E
Oli	15 Feb 1993	15.2°S, 172.8°E	20 Feb 1993	35.0°S, 175.1°W
Polly	25 Feb 1993	16.0°S, 158.0°E	9 Mar 1993	42.5°S, 169.0°W
Rewa	28 Dec 1993	9.5°S, 166.5°E	23 Jan 1994	40.6°S, 168.3°E
Sarah	19 Jan 1994	17.0°S, 170.5°E	4 Feb 1994	52.0°S, 157.5°W
Usha	24 Mar 1994	11.5°S, 157.5°E	4 Apr 1994	47.0°S, 172.0°W
Atu	11 Mar 1996	21.0°S, 168.0°E	18 Mar 1996	49.0°S, 171.5°W
Beti	21 Mar 1996	12.5°S, 170.9°E	2 Apr 1996	48.5°S, 175.2°W
Fergus	24 Dec 1996	13.1°S, 159.6°E	1 Jan 1997	52.0°S, 151.0°W
Drena	3 Jan 1997	13.6°S, 167.7°E	13 Jan 1997	53.0°S, 174.0°W
Freda	24 Jan 1997	20.0°S, 170.0°E	5 Feb 1997	53.5°S, 169.5°W
Nameless	23 Feb 1997	18.0°S, 159.2°W	2 Mar 1997	48.5°S, 164.5°W
Gavin	3 Mar 1997	8.8°S, 171.5°E	14 Mar 1997	48.0°S, 168.0°W

b. Empirical orthogonal function analysis

Following Harr et al. (2000) and Klein et al. (2000), EOF analysis (Joliffe 1986) of 500-hPa heights is used to identify characteristic midlatitude circulation patterns accompanying ET near 30°S (section 4) and extratropical regeneration (section 5). EOF analysis is commonly used to classify the variety of synoptic types in a particular region (e.g., Christenson and Bryson 1966; Kutzbach 1967; Richman 1981; Kidson 1994). The EOFs are computed from the temporal covariance matrices constructed from the 50 cases of ET during 1970–97. To facilitate comparison with Harr et al. (2000), we used a similar procedure to that study. Following Harr et al. (2000), normalization of the time series of 500-hPa heights with respect to the temporal standard deviation was not performed. This highlights the higher-latitude synoptic variability that we wish to characterize. The annual cycle was also retained as in Harr et al. (2000). Experimentation revealed that removing the annual cycle resulted in only small changes to the spatial eigenvector patterns. Evidently, intraseasonal circulation variability in the Southern Hemisphere (SH) dominates the smaller, more spatially coherent changes in the average circulation during the SH hurricane season (December to April).

Varimax rotation (Richman 1986) of the leading 10 principal components (PCs) is employed to isolate, as far as possible, single or dipole anomaly centers whose synoptic interpretation would be simplified. Rotation was accomplished by leaving the time series (the rotated PCs) mutually orthogonal, but relaxing the orthogonality of the spatial patterns (the EOFs). The number of components to rotate is somewhat arbitrary. A rotation of fewer components often results in overly complex patterns with inadequate regionalization while overrotation produces excessive regionalization (O'Lenic and Livezey 1988). Richman (1986) also found that spatial patterns of rotated eigenvectors are more robust with respect to sampling variations than their unrotated counterparts.

Geopotential height at 500 hPa was first interpolated onto a movable 31 × 31 Lambert conformal domain of size 3330 km × 3330 km centered on each storm. This domain was exactly centered on the minimum 850-hPa vorticity using bicubic splines. Vorticity at 850 hPa was used because of reduced flow distortion at this level near the rugged islands of New Caledonia and New Zealand. The EOF analysis was performed on the set of 50 fields extracted at the time when each storm was closest to 30°S. The temporal coefficients, or principal components for each spatial eigenvector pattern were then used to produce positive and negative composites of various fields by averaging cases having PC amplitude more than one standard deviation above and below the temporal mean. These composites would be expected to be more meaningful and representative of actual synoptic cases than composites obtained from simple averages across a variety of diverse synoptic types.

3. Extratropical transition onset

The composites of Sinclair (2002) suggested that southwest Pacific TCs commence ET earlier than their NH counterparts. As noted earlier, the time of ET onset is seldom recorded in the NZMS database. Here, for the first time, the location of southwest Pacific ET onset is identified for a large number of TCs using an objective diagnostic technique.

a. Definition of transition onset

Following EH, the time of transition onset is identified from the asymmetry in the thermal field. This was diagnosed by first identifying the average 600–925-hPa thermal wind vector averaged over a 500-km radius circle. The warm minus cold asymmetry was then determined from the 600–925-hPa thickness field as

$$B = (\overline{Z_{600} - Z_{925}})_{\text{warm}} - (\overline{Z_{600} - Z_{925}})_{\text{cold}}, \qquad (1)$$

where Z_{600} and Z_{925} are the 600- and 925-hPa heights and the overbars indicate the areal means over the semicircles on the warm and cold side of the average thermal wind vector. This is identical to the method of EH except here asymmetry is computed left minus right relative to the thermal wind vector rather than to the storm translation vector, as in EH. Calculations based on the method of EH yielded widely fluctuating B values, especially where the direction of motion was varying. Furthermore, it is common for SH TCs to move nearly at right angles to the thermal wind (e.g., Fig. 10 of Sinclair 2002), resulting in smaller values of B. North Atlantic transitioning TCs seldom approach the baroclinic zone head-on (J. Evans 2003, personal communication), as they are typically recurving ahead of an approaching trough, resulting in a track toward the east-northeast that often parallels the Gulf Stream (Hart and Evans 2001). The method used here based on the thermal wind vector yielded smoothly varying values of B for most tracks. Following EH, the onset of ET was judged to have begun at the start of the period when B exceeded 10 m in three or more successive 12-hourly analyses.

For most storms, the transition to an asymmetric structure as defined by B was well defined and rapid, with near-zero values of B typically increasing to an average of around 30 m following ET onset, with about a third of storms attaining B values in excess of 50 m. These results for the evolution of B are quite similar to those of EH for the North Atlantic.

Occasionally, the increase in B was transient or irregular. For example, TC Patsy interacted with two midlatitude systems (Sinclair 1993a). The first system passed to the poleward side of Patsy, shearing off the symmetric upper-level anticyclonic circulation and stranding Patsy as a shallow, weakening, warm-cored vortex. Vertical shear was present above 500 hPa but low-level moisture and thermal fields retained much of the original TC symmetry. Interaction with a second midlatitude trough and associated upper jet resulted in modest extratropical regeneration and the progressive appearance of cold and warm front–like features, with these changes occurring over a period of several days. Corresponding values of B computed for Patsy revealed one short-lived ($<$24 h) pulse of $B > 10$ m for the first trough interaction and a second more-prolonged period of B ranging between 10 and 15 m (i.e., only just fulfilling the threshold for ET onset). A few other ET cases in the sample exhibited similar complexity in their evolution.

b. Climatology of ET onset

The tracks of all 50 TCs, with the diagnosed locations of ET superimposed, are shown in Fig. 1. This shows that ET onset most commonly occurs between 20° and 30°S, with an average latitude of ET onset of 24.3°S. Comparison with the similar figure from EH (their Fig. 1) reveals that ET onset in the southwest Pacific occurs at markedly lower latitudes than in the North Atlantic, where ET occurs most frequently between 35° and 45°N, as also shown by Hart and Evans (2001) using U.S. National Hurricane Center (NHC) estimates of ET onset.

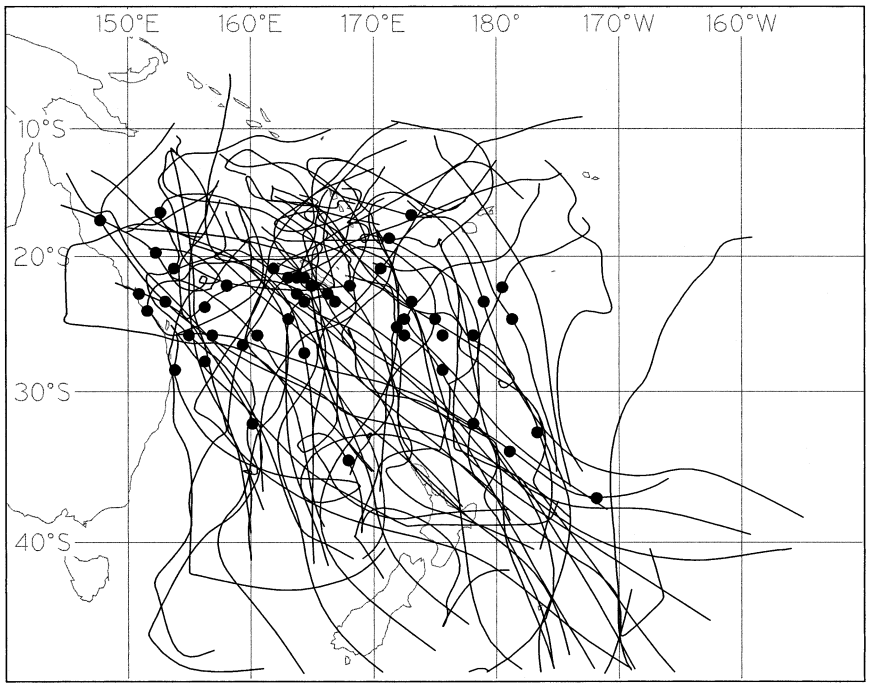

FIG. 1. Tracks for the 50 tropical cyclones included in this study. Location of extratropical transition onset (heavy dot).

Another difference is that the tracks in Fig. 1 are much more irregular than those shown in both Hart and Evans (2001) and EH. This explains the need to here reference the calculation of B to the average thermal wind rather than to the highly variable track direction as in EH.

Table 2 shows the average latitude of ET onset, stratified by month. Onset of ET occurs at an average latitude of 23.3°S for December and April, and 25.2°S for February, a variation of less than 2° latitude during the TC season. This small variation is statistically insignificant at the 95% confidence level. In comparison, average latitudes for ET onset in the North Atlantic range between 36°N in June and November to 44°N in July (Hart and Evans 2001). Sixteen northwest Pacific tropical storms and typhoons during 1971 became extratropical at an average latitude of 32°N (Brand and Guard 1978). However, when six winter and spring storms were excluded, the average latitude of ET is 41°N. Clearly, southwest Pacific TCs commence ET around 15° of latitude nearer the equator than their NH counterparts.

To identify the synoptic setting for ET onset, composites were constructed for the nine instances where ET commenced equatorward of 21°S (Figs. 2a,c) and the eight instances where ET onset occurred poleward of 28°S (Figs. 2b,d). These composites were prepared by first remapping each TC onto a moveable 31 × 31 grid centered on the minimum 850-hPa vorticity, as explained in the previous section. For both latitude belts, ET onset occurred with the approach of a midlatitude trough, with the TC entering the equatorward flank of a midlatitude baroclinic zone. Both composites exhibit marked thermal and ascent asymmetry, with the TC moving south into the equatorward entrance region of an upper jet. Although average 850-hPa temperatures near the TC core were around 16.5°C in both composites, the higher-latitude composite showed the TC to be within a strong thermal ridge with cooler air east and west of the center (Fig. 2b), whereas the low-latitude composite showed a thermal trough near the TC (Fig. 2a).

In both composites, the TC already was absorbed into the midlatitude trough system at the time of ET onset, with marked asymmetry of the upper circulation. Clearly, the present definition of ET onset requires the TC to encroach on the equatorward flank of a lower-tropospheric baroclinic zone. This appears to happen at some stage following absorption of the TC into the midlatitude trough circulation. Presumably, different definitions of ET onset would yield different results. For example, a definition based on upper-flow asymmetry could yield a slightly earlier diagnosis of ET onset. Sin-

TABLE 2. Average latitude of extratropical transition onset, by latitude. Uncertainty is expressed at the 95% confidence level.

Month	Mean lat (°S)
Dec	23.3 ± 2.1
Jan	24.9 ± 3.0
Feb	25.2 ± 3.8
Mar	24.1 ± 2.0
Apr	23.3 ± 5.7

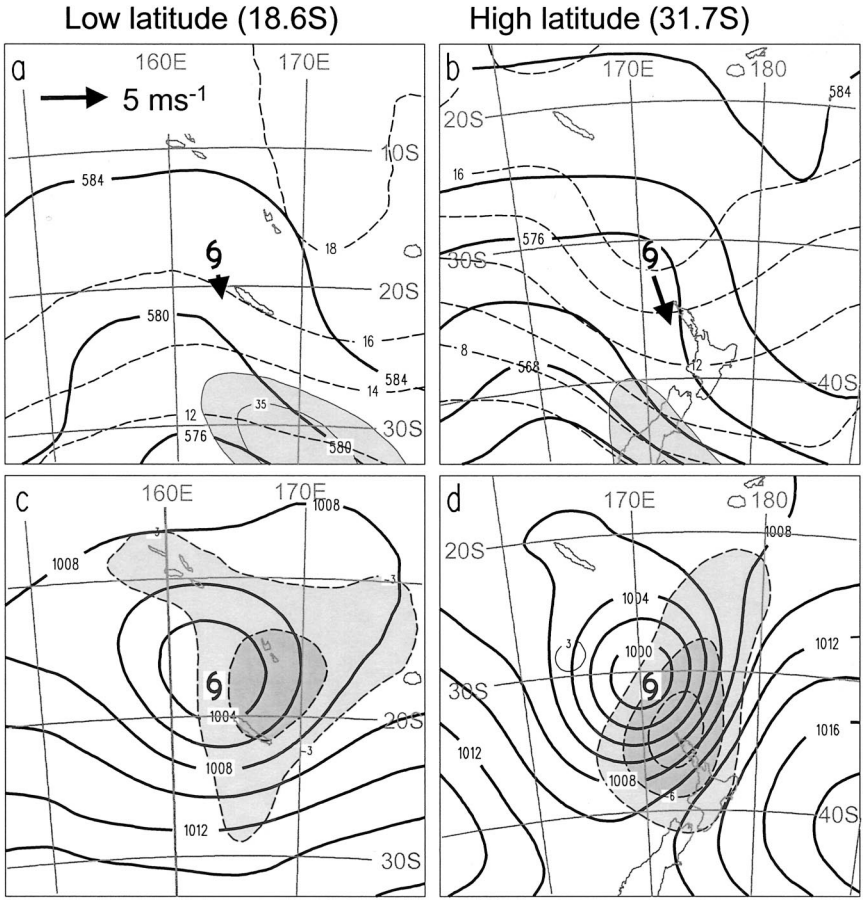

FIG. 2. Composites for (a), (c) nine cases where ET onset occurred north of 21°S and (b), (d) eight cases south of 28°S. (a), (b) 500-hPa height (solid, every 4 dam) and 850-hPa temperature (dashed, every 2°C), and 250-hPa isotachs (thin, every 5 m s^{-1} from 35 m s^{-1}) with values above 35 m s^{-1} (45 m s^{-1}) having light (darker) shading. (c), (d) MSL pressure (solid, every 2 hPa), and 700-hPa vertical P velocity, ω, every 3 hPa h^{-1}, with positive (negative) values thin solid (dashed) and the zero contour omitted. Ascent regions ($\omega < -3$ hPa h^{-1} and -6 hPa h^{-1}) are shaded. Vectors indicate avg storm motion, while the hurricane symbol marks the surface location of the storm center.

clair (2002) noted marked upper-flow and ascent asymmetries as early as 15°–20°S. Often, the low-level flow retains much of the original thermal and flow symmetry from the parent hurricane long after the symmetric upper-level warm core and cloud shield has been sheared off (Sinclair 1993a). Thus, the present definition probably yields a late diagnosis of ET onset compared with (say) satellite imagery that would detect asymmetry in the upper-level cloud shield before any baroclinic deformation of the low-level thermal fields. This is confirmed by Table 1 of EH, which compares the objective measure with the NHC best track declaration time based largely on satellite imagery. On average, the objective measure declared ET onset around 8 h after the NHC.

4. Characteristic midlatitude circulation features during extratropical transition

In this section, EOF analysis of 500-hPa heights is used to identify commonly recurring midlatitude circulation types for TCs undergoing ET near 30°S. In the previous section, it was shown that most TCs undergoing ET in the southwest Pacific basin start to interact with the baroclinic westerlies between 20° and 30°S, with 44 out of 50 TCs having commenced ET by 30°S (Fig. 1). The strong zonal symmetry of the SH circulation (see, e.g., Fig. 5 of Sinclair 2002) also means that there is little longitudinal variation in average midlatitude circulation characteristics. Here, we take advantage of the zonal symmetry and identify the synoptic variability at 30°S as these ex-TCs enter New Zealand waters.

Table 3 shows the proportion of variance associated with the first 10 unrotated EOFs. Assuming that the 50 cases of ET in Table 1 are independent, the criterion of North et al. (1982) yields a fractional uncertainty for each eigenvalue, $\delta\lambda/\lambda_i$, of ± 0.19, expressed as absolute errors in Table 3. A straight-line fit to $\log(\lambda_i)$ versus EOF number i explained over 99% of the variance for

TABLE 3. EOF number and % of variance associated with the first 10 EOFs, with the absolute uncertainty from the test of North et al. (1982) included.

REOF	*H* 500
1	45.7 ± 12.9
2	12.1 ± 3.4
3	12.1 ± 3.4
4	9.9 ± 2.8
5	6.1 ± 1.7
6	5.2 ± 1.5
7	2.0 ± 0.6
8	1.8 ± 0.5
9	1.7 ± 0.5
10	1.5 ± 0.4
1–10	98.6

EOFs 11–20, indicating these to be noise (Craddock and Flood 1969). When this logarithmic fit was extrapolated back to the lower-numbered EOFs, just EOFs 1–8 are distinguishable from the uncertainty in Table 3. These leading nonnoise EOFs explained a total of around 97% of the variance.

Each rotated PC was correlated with a small set of selected storm properties mostly related to track and intensity change. These were 850-hPa vorticity at the storm center (center vorticity), center vorticity change (computed as a 24-h centered difference of 850-hPa center vorticity), *U*- and *V*-components of storm translation, longitude, and the Southern Oscillation index (SOI). To identify if any of the rotated EOFs represented circulation variations due to the annual cycle, the PCs were also correlated with a variable $X = |M - 2|$ representing months from February (the warmest month), where M is month. For December, M was 0. No statistically significant correlations with X (or M) were found for any PC. Statistically significant correlations ($|r| > \sim 0.3$) from this set are listed in the bottom left of the eigenvector plots. No statistically significant correlations were found for longitude, season, or SOI, for any of the PCs. Experimentation revealed that rotated PCs were better correlated with TC motion and intensity than unrotated PCs, further justifying the use of rotation.

a. REOF-1

The spatial eigenvector pattern for the first rotated EOF, REOF-1, (Fig. 3a) is monopolar, with the center of action located about 600 km south of the TC. This EOF, explaining 46% of the variance amongst the 50 cases of ET, represents variations in the strength of the westerlies in which the TC is embedded. Positive (negative) excursions of PC-1 represent high (low) 500-hPa heights to the south. PC-1 positive patterns where PC-1 is more than 1 standard deviation above the mean are called *high south* patterns while PC-1 negative patterns (PC-1 at least 1 standard deviation below the mean) are called *low south*. There were nine cases in the high south and seven in the low south composites. As would be expected, this PC is highly correlated with the *u* component of storm translation ($r = -0.76$) and with overall translation speed ($r = -0.60$). However there was no significant correlation of the PC with storm intensity as measured by central 850-hPa vorticity.

As noted earlier, no statistically significant correlations were found with season (X or M), suggesting that the patterns in Fig. 3 can occur at any month during the TC season. In similar studies for the NH by Harr et al. (2000) and Klein (1997), the two leading eigenmodes were found to represent seasonal variations in the circulation patterns and so were not considered further. Here, case-to-case variability in the strength of the westerlies masks the much smaller SH annual cycle. The average 500-hPa wind speed in the region bounded by 15° and 40°S and 150°E and 150°W varies only slightly during the SH hurricane season, from a minimum of 10 m s^{-1} in February to a maximum of 13 m s^{-1} in April (www.cdc.noaa.gov). The variation in background 500-hPa winds between the high south and low south composites in Figs. 3b and 3c is clearly much larger than this. Experiments with the annual cycle removed caused only slight changes to the spatial eigenvector pattern in Fig. 3a and fraction of explained variance for PCs 2 and 3 (Table 3). We conclude that, unlike the NH, the contribution to synoptic variability from the seasonal cycle is small for the southwest Pacific Ocean basin.

In the SH, the dominant mode of circulation variability on time scales from intraseasonal to interannual represents zonally symmetric fluctuations in the strength and location of the midlatitude westerlies (e.g., Kidson 1988; Karoly 1990). Thus, it is not surprising that the leading mode of synoptic variability accompanying ET near 30°S also features variations in the background height gradient (Fig. 3). Clearly some TCs enter middle latitudes during periods of enhanced height gradients while others do so during episodes of relaxed background height gradients. Hartmann (1995) suggested that these variations in the zonal background flow result in different evolution of baroclinic waves.

The high south composites (Figs. 3b,d) show the surface center moving almost due south in the region just east of a 500-hPa cutoff low. There is a 500-hPa ridge to the south, and the low has a warm core structure, with warmest air located just northeast of the low and cooler air wrapping about the western sector of the low, suggesting that extratropical transformation is well under way. Baroclinity is marked near and east of the center, with the suggestion of a warm front–like feature in this region. The high south surface chart (Fig. 3d) shows a strong high located southeast of the low. Strongest ascent is east of the low with frontogenesis east of the ascent within a zone of confluence within the baroclinic zone. The ascent maximum is located slightly to the left of the storm motion. The high south synoptic signature in Fig. 3d is similar to the ''cradled'' classi-

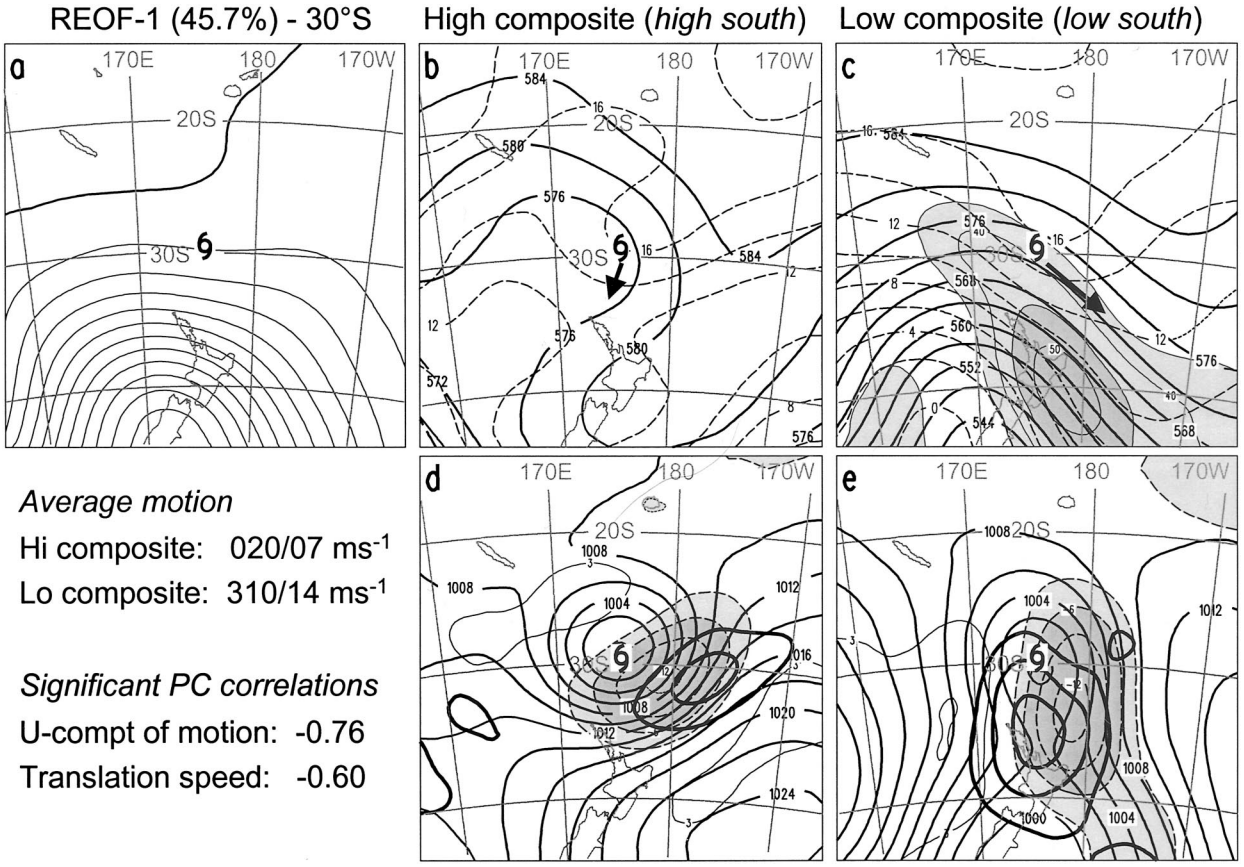

FIG. 3. (a) First rotated EOF eigenvector pattern for 500-hPa height variations at 30°S. (b) High-composite 500-hPa height (solid, every 4 dam) and 850-hPa temperature (dashed, every 2°C), and 250-hPa isotachs (thin, every 5 m s^{-1} from 35 m s^{-1}) with values above 35 m s^{-1} (45 m s^{-1}) having light (darker) shading. (c) As in (b) except low composite. (d) High-composite MSL pressure (solid, every 2 hPa), 850-hPa frontogenesis (thick solid, every 5K m^{-6} day^{-1}), computed as in Petterssen (1936), and 700-hPa vertical P velocity, ω, every 3 hPa h^{-1}, with positive (negative) values thin solid (dashed) and the zero contour omitted. Ascent regions ($\omega < -3$ hPa h^{-1} and -6 hPa h^{-1}) are shaded. (e) As in (d) except low composite. (b), (c) Vectors illustrate average storm motion, indicated quantitatively in the bottom left, along with other significant PC correlations. The hurricane symbol marks the surface location of the storm center.

fication of Foley and Hanstrum (1994), which also featured a surface high to the southeast (their Fig. 5a).

The low south composite (Fig. 3c) features a vigorous 500-hPa trough to the south, with the TC moving rapidly southeast at double the speed of the high south composite low. The surface center is located beneath the equatorward entrance region of a strong upper jet with a broad band of baroclinity beneath. The surface pattern (Fig. 3e) features a strong trough to the south and a meridional band of ascent located slightly to the right of the storm motion. The thermal gradient and associated frontogenesis is stronger than for the high composite, and is more meridionally oriented. It is particularly focused on the col region south of the surface low and west of the strongest ascent. The low appears to be in the process of merging with the trough to the south, making this synoptic signature similar to the ''captured'' classification of Foley and Hanstrum (1994). As will be shown later, there is also some redevelopment, as was the case with Foley and Hanstrum's (1994) captured examples.

Tracks for the nine high south and seven low south cases are shown in Fig. 4. The high south (REOF-1 positive) cases (Fig. 4a) feature mostly meridional tracks whereas the low south cases (Fig. 4b) featured more zonal motion south of 25°S. Some of the low south cases feature sharply recurving tracks near 20°–25°S whereas the high south cases have more consistent poleward motion.

Central vorticity and pressure traces (Fig. 5) are used to identify trends in storm intensity. These are composited so that 0 h corresponds to the time when each storm was at 30°S. Sinclair (2002) showed that central vorticity is a better measure of true TC intensity than central pressure. This is because it is common for central pressures of poleward-moving SH cyclones to fall without a corresponding increase in the cyclonic circulation (Sinclair 1997). The vorticity traces showed that on average, the slower-moving high south (REOF-1 positive) storms (Fig. 5a) had largely completed a 2-day period of intensification prior to reaching 30°S, with weakening and filling beyond 30°S (the zero line in Fig. 3). How-

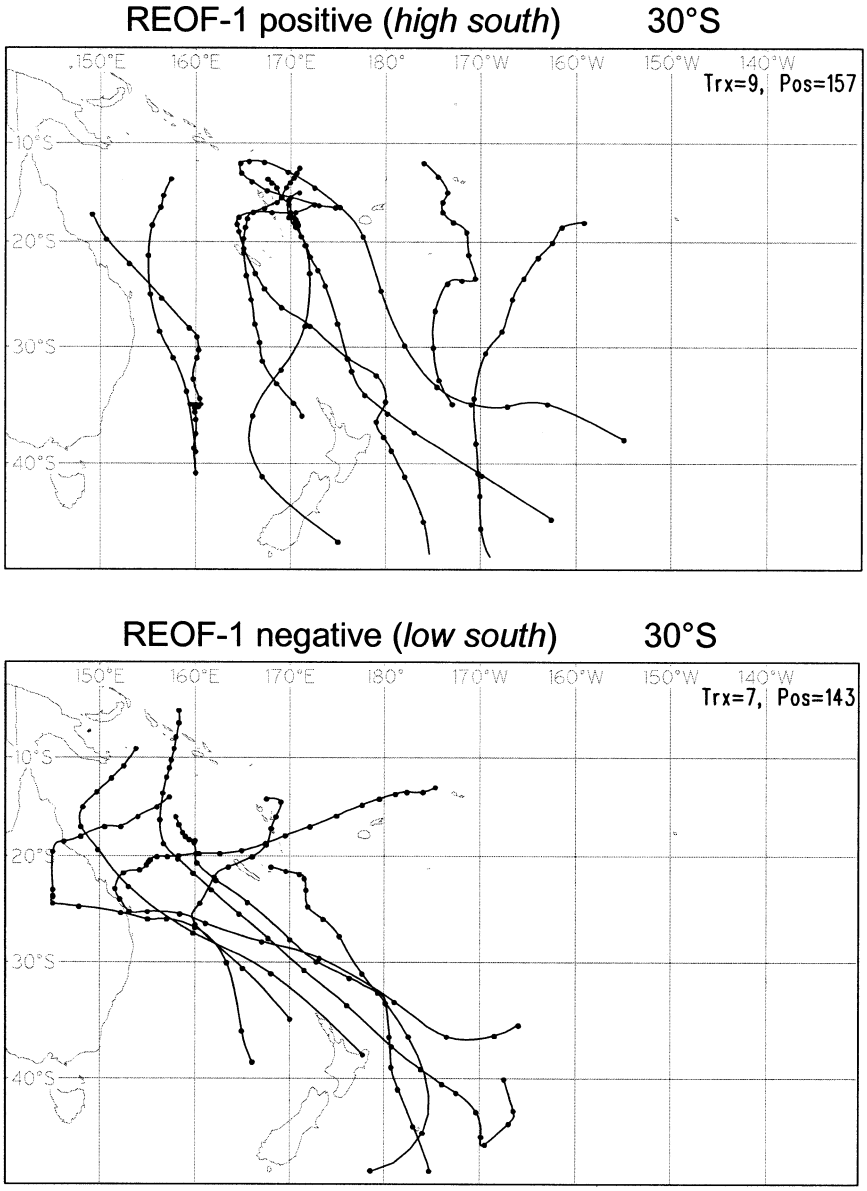

FIG. 4. Tracks of tropical cyclones having rotated PC-1 (a) more than 1 std dev above the mean and (b) less than 1 std dev below the mean. Dots indicate 12-hourly positions.

ever, the low composites (Fig. 5b) exhibited progressive intensification at 30°S and in the 24 h following.

The 48-h composite evolution of the storms included in the low composites for REOF-1 as they pass 30°S is shown in Fig. 6. Twenty-four hours prior to reaching 30°S (Figs. 6a,d) the composite low is moving poleward toward a 250-hPa jet stream, with a meridional band of ascent to the southeast, with strongest baroclinity south of the storm. Already, at this stage, the TC has lost its outflow pattern at 200 hPa (not shown), consistent with the finding of Sinclair (2002) that southwest Pacific TCs lose their symmetric outflow pattern by 25°S. On reaching 30°S, there is cooling west of the low (Fig. 6b) that is located beneath the equatorward entrance of the upper jet, with strengthening of the surface circulation, the ascent field (Fig. 6e), and the baroclinity south of the storm. Twenty-four hours later, the composite surface low crosses to poleward of the upper jet (Fig. 6c), with marked cooling west of the low, strengthening the thermal gradient just west of the low and producing a second zone of cold frontogenesis north of the center. The strengthening low-level circulation appears to contribute to this cold frontogenesis (Fig. 6f). It is likely that the appearance of a jet streak northwest of the center (Fig. 6c) was an in situ response to this frontogenesis. The appearance of this second jet results in a double upper-jet signature. Another factor possibly contributing to the split jet signature is erosion of the primary jet by com-

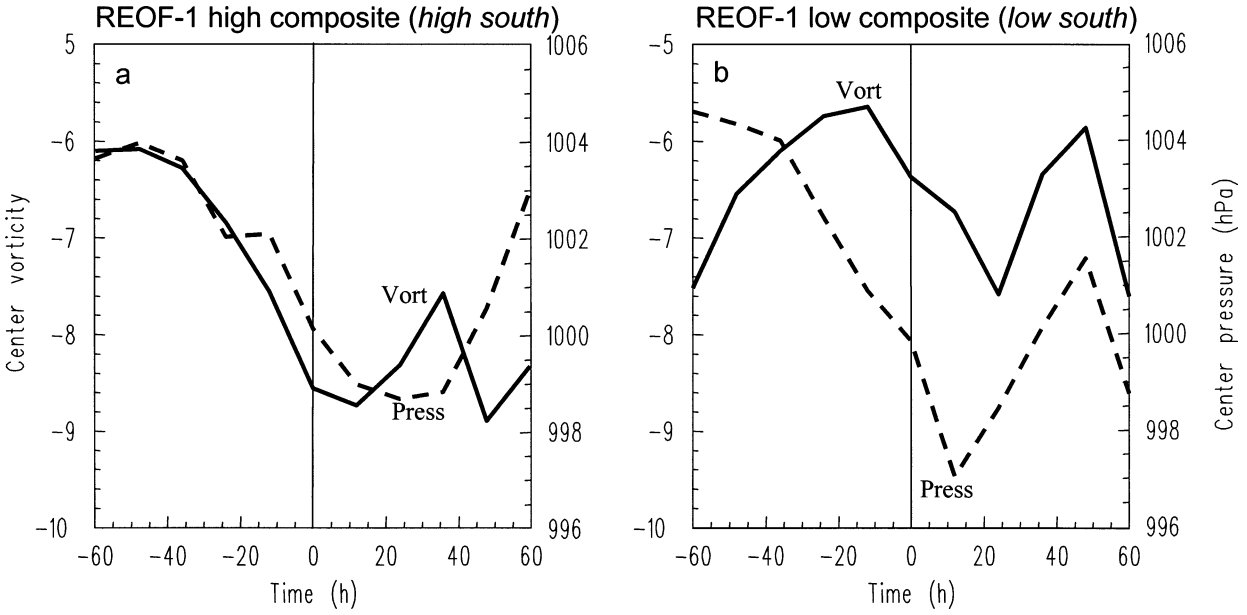

FIG. 5. (a) High- and (b) low-composite central vorticity (solid) and central MSL pressure (dashed) time series, for rotated EOF-1. Center vorticity (10^{-5} s^{-1}) is indicated at left and central pressure (hPa) at right, and time is hours since each storm was at 30°S.

bined warm advection and diabatic heating within the ascent region southeast of the low as the storm center crosses to the poleward side of the upper jet. The observed ridging and weakening of the flow above this region is evidence of this process.

Thermal gradients in Figs. 6a–c rotate, tighten, and become more meridional in orientation during this 48-h period in a manner similar to that described by Harr and Elsberry (2000) for decaying western North Pacific TCs that undergo reintensification as extratropical cyclones. This evolution of surface and upper-air features described here also mimics that of the capture events described by Foley and Hanstrum (1994). In contrast, the evolution of the high composites (not shown), features a slow weakening (see Fig. 5a) as the composite low progresses slowly south-southwest along the western periphery of an intense high.

In summary, this first eigenvector pattern, explaining nearly half the midlatitude variability, is similar to the subjectively derived cradled and captured classifications described by Foley and Hanstrum (1994). The present high south category matches their cradled category and exhibits steady poleward movement into a region of environmental easterly flow. High south cyclones usually commence weakening south 30°S (Fig. 5a). The low south, corresponding to Foley and Hanstrum's (1994) captured classification, features a strong meridional cold front and low pressure to the south, with strongest baroclinity southwest of the storm. These storms typically intensify (Fig. 5b) after crossing 30°S and accelerate to the southeast, with average translation speeds double those of the high south storms. Foley and Hanstrum (1994) observed that captured storms commenced to accelerate to the southeast when the surface cold front approached from the southwest to within an average distance of 1700 km from the surface low center. Based on previous studies (e.g., Brand and Guard 1978; Hanley et al. 2001), significant interactions between systems with more than 1700-km separation are unlikely.

b. REOF-2

The second rotated eigenvector pattern is bipolar (Fig. 7a), with out of phase centers of action southwest and southeast of the surface low center. This EOF explains 12% of the variance. No statistically significant correlations were found with track or intensity parameters. High composites exhibit a 500-hPa ridge southwest of the center and a trough to the south or southeast (Fig. 7b) while low composites have a trough to the southwest and ridging to the southeast (Fig. 7c). By analogy with Harr et al. (2000), we refer to these cases as *southeast* for the high composite and *southwest* for the low composite, the title referring to the direction of the dominant midlatitude trough. These are the SH analogues respectively of Harr et al.'s northeast and northwest patterns so far as the broadscale location of the primary midlatitude trough is concerned. Taken together, the main difference between the high and low composites is that the trough in the southeast cases (high composite) tilts westward and equatorward (analogous to positive tilt in the NH) and eastward in the northwest cases (like negative tilt in the NH). For the purpose of comparison with NH studies, we will refer to the westward tilt in

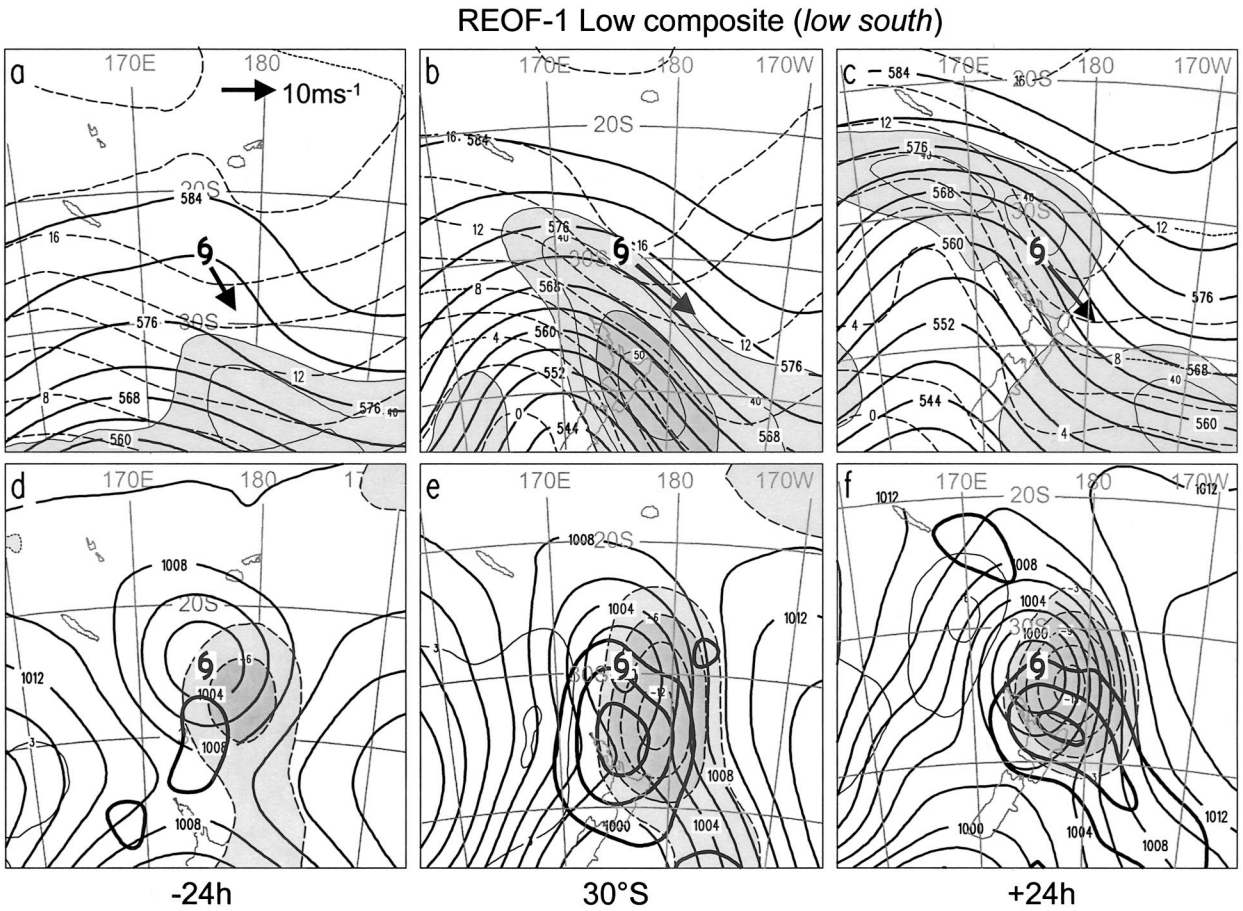

FIG. 6. Composites of the evolution of low south storms, for (a), (d) 24 h before reaching 30°S, (b), (e) at 30°S, and (c), (f) 24 h after passing 30°S. (a)–(c) Fields are 500-hPa height (solid), 250-hPa isotachs (shaded), and 850-hPa temperatures (dashed); (d)–(f) MSL pressure (solid), 850-hPa frontogenesis (thick, solid), and vertical P velocity (shaded). Units, contour, and shading intervals as in Fig. 1. Vectors illustrate avg storm motion while the hurricane symbol marks the surface location of the storm center. (b), (e) Reproduced from Fig. 3.

the southeast cases as positive and the eastward tilt in the southwest case as negative.

Cyclones moving into the positively tilted southeast pattern (Figs. 7b,d) are moving toward the equatorward entrance region of an upper jet. Baroclinity and frontogenesis are most marked in the poleward sector, with the low moving directly toward the strongest ascent. Composite pressure and vorticity traces (Fig. 8) reveal that storms moving into the southeast pattern undergo considerable intensification (Fig. 8a) after crossing 30°S whereas those associated with the negatively tilted southwest pattern weaken (Fig. 8b). Successive composite charts (Fig. 9) for the intensifying southeast storms reveal a progressive increase in ascent, baroclinity, and frontogenesis (Figs. 9d–f), with the composite storm crossing to the poleward side of the upper jet (Fig. 9c) 24 h later when there is again evidence of a double upper-jet configuration similar to that in Fig. 6c. At this time the storm is continuing to reintensify (Fig. 8a).

Storms moving into the negatively tilted southwest pattern (Figs. 7c,e) feature upper winds <35 m s^{-1}, and weaker baroclinity and frontogenesis. The vorticity and pressure traces (Fig. 8b) show that these low composite southwest storms are weakening. The evolution of the southwest composites (not shown) features a weakening low eventually absorbed into the northerly flow ahead of the trough (not shown). This weakening trend is not surprising considering the weaker upper jet and baroclinity.

This second spatial eigenvector pattern can be compared with the northeast and northwest patterns of Harr et al. (2000). Klein et al. (2000) noted that storms moving into the northwest pattern tended to intensify more rapidly and take a meridional track while storms in the northeast pattern intensified only slowly with more zonal motion. Here, there was little difference between tracks for southeast versus southwest storms (not shown) and storms moving into the southeast pattern featured the larger development rates. Harr and Elsberry (2000) compared the rapidly deepening northwest pattern example of Typhoon David with a weakening northeast case (Opal) and attributed the intensification of David to a pattern of rotational frontogenesis that rein-

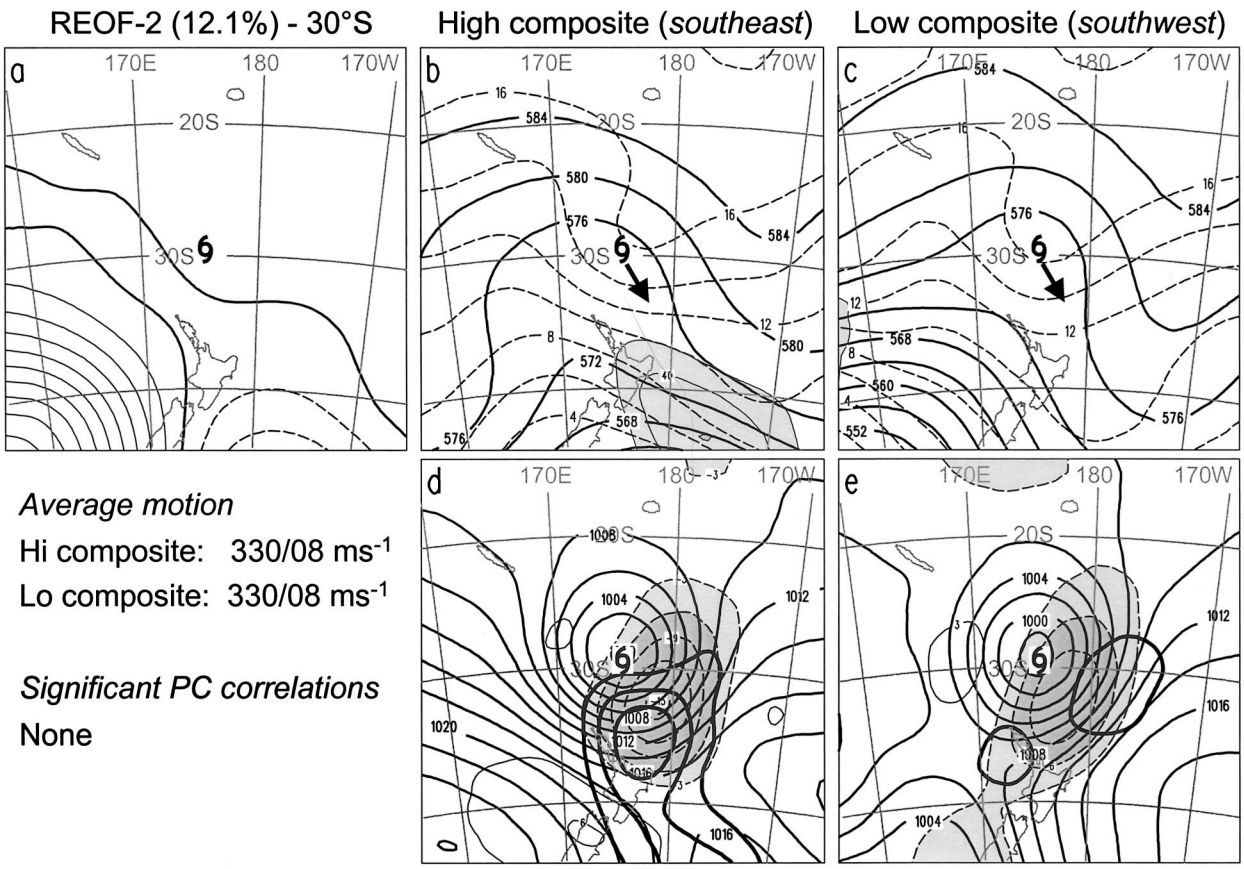

FIG. 7. As in Fig. 3 except for second rotated EOF eigenvector pattern.

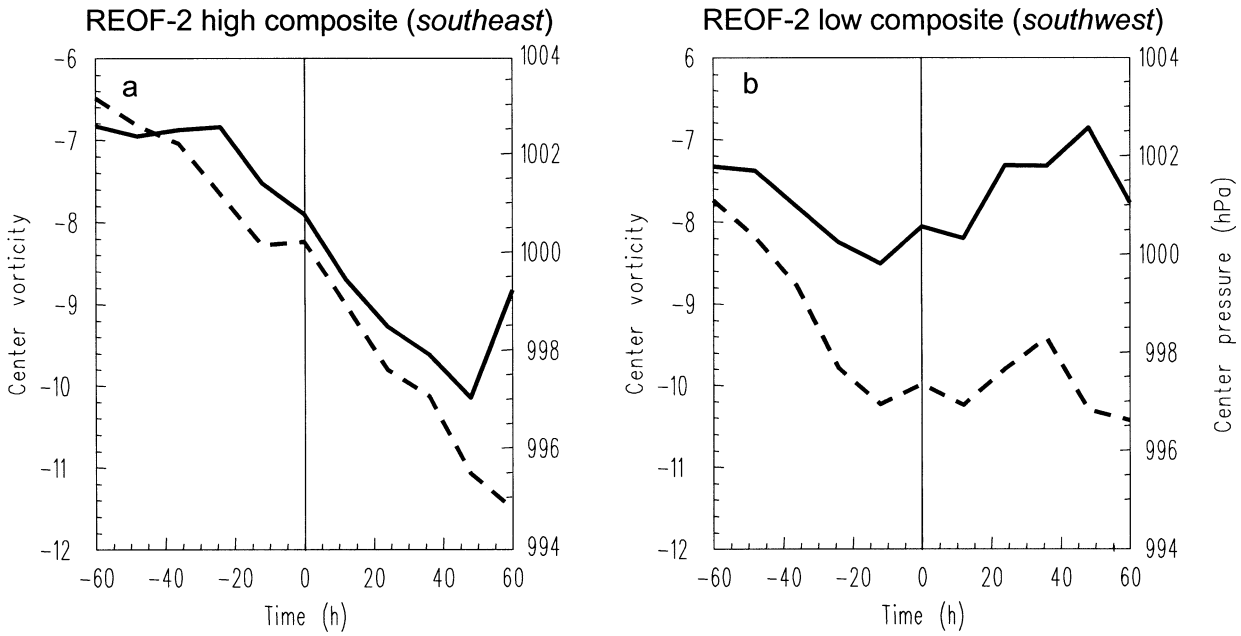

FIG. 8. As in Fig. 5 except for rotated EOF-2.

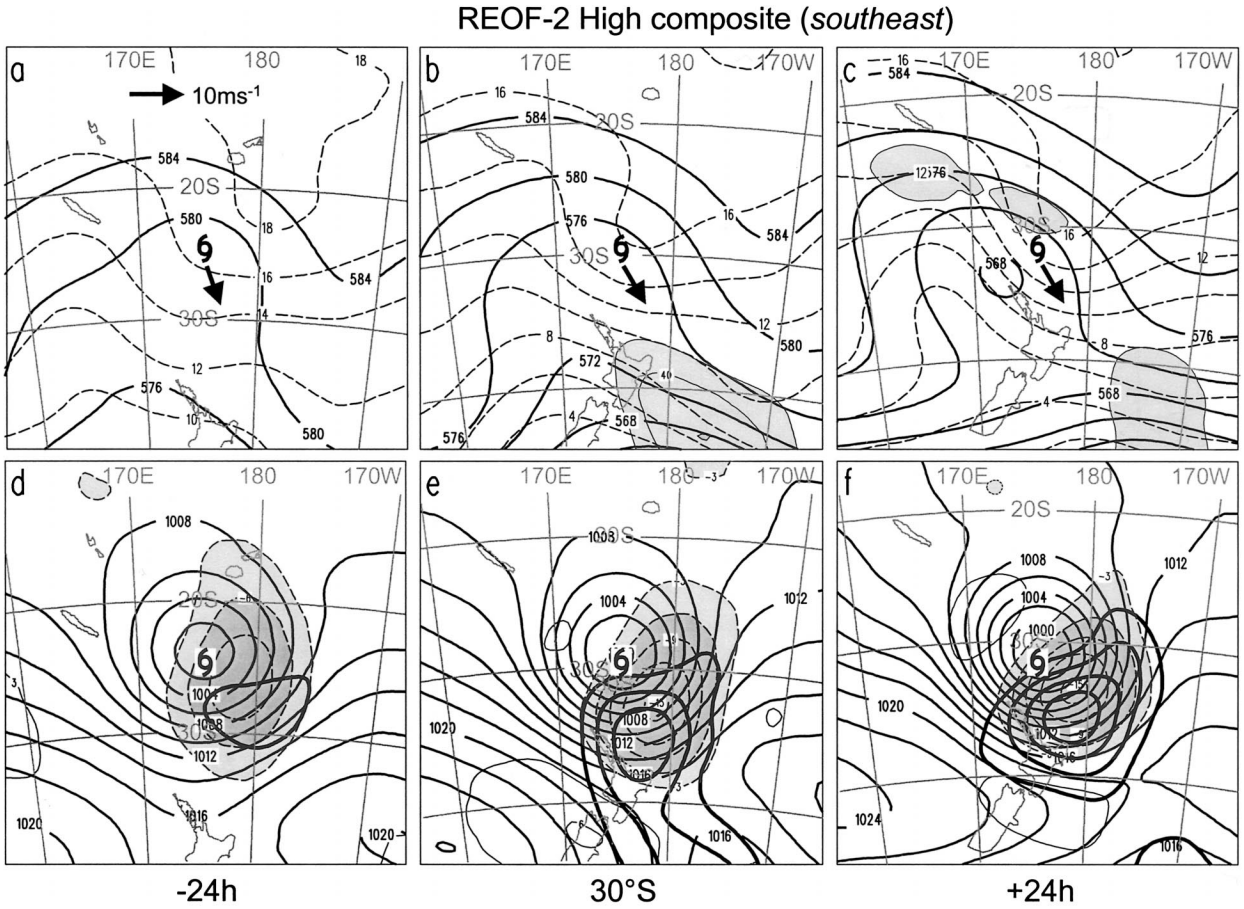

FIG. 9. As in Fig. 6 except for southeast storms.

forced the dynamical support for coupling with the midlatitude trough.

Another factor evident in the study of Harr and Elsberry (2000) but not directly mentioned there, was the upper jet stream configuration and strength of the downstream upper ridge. Their more vigorous negatively tilted northwest case featured stronger upper flow with a more potent downstream ridge, resulting in increased cyclonic vorticity advection (CVA) between the trough and the stronger downstream ridge (cf. their Figs. 5a and 14a). Although the southwest case here had the similar tilt and broadscale synoptic orientation relative to the primary circulation center, there was no strong upper jet. Figure 10 compares the jet-level environment for the two composites. The southeast cases (Fig. 10a) exhibit stronger upper flow, downstream ridging, and strengthened vorticity gradient resulting in increased CVA and stronger development rates. In addition, the upper-level CVA is occurring in a more anticyclonic environment near the equatorward entrance region of a downstream upper jet, resulting in more efficient generation of divergence. In comparison, the southwest composite (Fig. 10b) exhibits weaker CVA because of smaller wind speeds and weaker downstream anticyclonic vorticity. There, the primary influence of the midlatitude trough is to steer the TC poleward, but the primary upper-level CVA and the strongest upper jets are well to the west.

In the studies of Harr et al. (2000), Klein et al. (2000), and Harr and Elsberry (2000), the primary trough accompanying reintensifying storms was west of the TC (northwest pattern). Here it was to the east (southeast pattern). Evidently, the locations of more distant broadscale primary circulation features or the tilt of the trough itself are less important to development than details of the circulation near the low itself, particularly at the jet level. Here, the presence of a stronger upper-level flow and a stronger downstream ridge for the southeast cases increases the local magnitude of storm-relative CVA at the jet level above the storm, leading to storm intensification. Bosart and Lackmann (1995) found that upper-level ridging downstream of a rather weak midlatitude disturbance was a contributing factor to the reintensification of Tropical Storm David over the eastern United States. In simulations of ET over the western North Pacific, Ritchie and Elsberry (2003) found that a weak midlatitude trough interacting with a TC had as much potential to intensify as with a stronger trough.

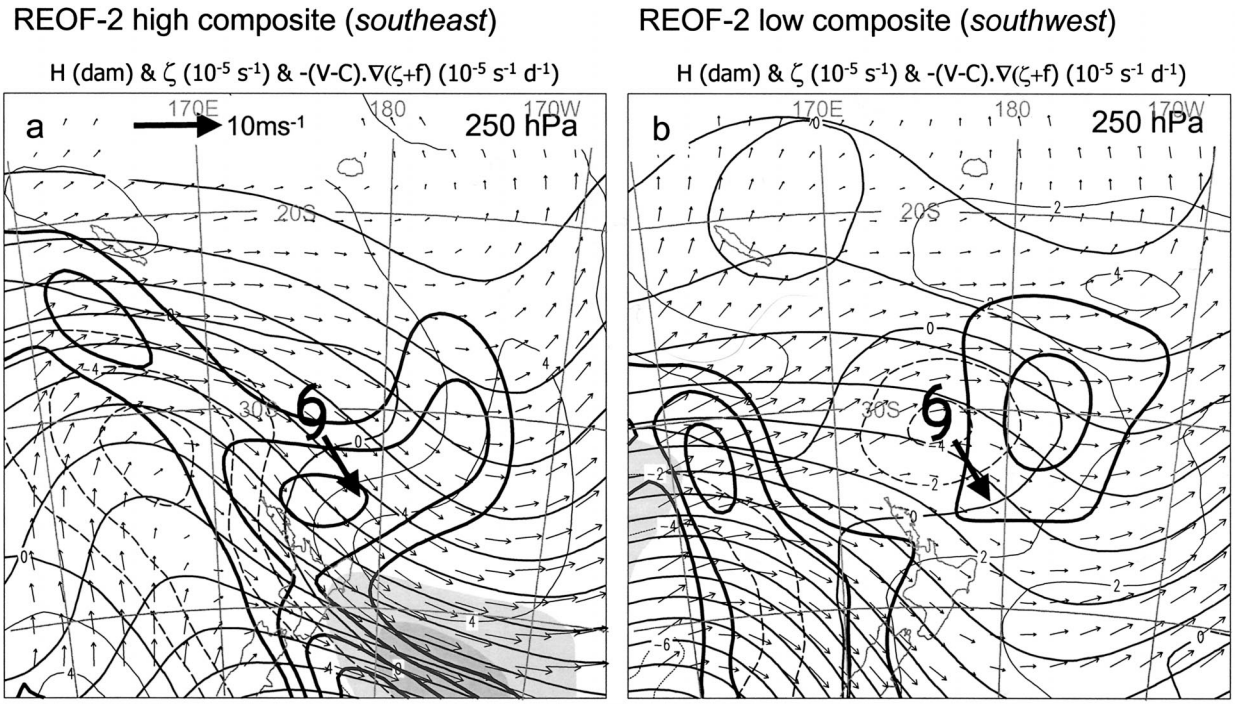

FIG. 10. Fields at 250 hPa, for (a) southeast cases and (b) southwest cases. Heights (solid, every 10 dam), storm-relative winds, $\mathbf{V} - \mathbf{C}$ (arrows), isotachs (values 30 and 35 m s^{-1} shaded), relative vorticity [every 2×10^{-5} s^{-1}, values > 0 (thin solid), < 0 (dashed), and the zero contour (solid)], and cyclonic (negative) values of storm-relative vorticity advection by the storm-relative wind (thick solid, every 4×10^{-5} s^{-1} day^{-1}). The hurricane symbol marks the surface location of the storm center while the heavy vector indicates avg storm motion.

Addition of the TC to the simulations resulted in a stronger jet outflow and enhanced upper-level divergence. In Fig. 10a, the more rapid development of the southeast cases also appears to be related to a more favorable environment for upper-level divergence near the equatorward entrance region of the upper jet (Fig. 7b). This is also similar to the favorable distant interaction described by Hanley et al. (2001), where an upper PV maximum approaches to within 1000 km from the west and development occurs under the equatorward entrance region of the upper jet in such a way that the TC and the upper jet mutually reinforce each other.

c. *REOF-3*

Since REOFs-2 and 3 each explain a similar amount of variance (Table 3), the third rotated eigenvector pattern and associated high and low composites are shown (Fig. 11) for completeness. This third eigenvector pattern represents fluctuations in the strength of the 500-hPa vortex, with high composites corresponding to a stronger 500-hPa vortex (Fig. 11a) and a stronger surface low (Fig. 11d). Not unexpectedly, the associated PC is correlated with central vorticity. The stronger high composites feature a higher degree of cool air circulation into the northwest sector of the storm (Fig. 11b), but with weaker overall baroclinity. Ascent and frontogenesis magnitude appear to be similar for the two composites (Figs. 11d,e).

Some experimentation was performed to determine the robustness of the patterns shown in this section. Randomly removing one or two cases from the set of storms had very little impact on the synoptic signatures suggested in Figs. 3, 6, 7, 10, and 11. Removal of the annual cycle also had minimal impact, as noted earlier. For these experiments, the only impact was that the order of patterns 2 and 3 (in terms of explained variance) was swapped in some cases. Such degeneracy between patterns can imply a possible relationship between patterns, often a progression from one to the other. This is precluded here, since the PCs are uncorrelated, making the storms represented by different EOFs mutually exclusive.

5. Extratropical reintensification

During the first stage (transformation) of ET, the TC undergoes structure changes as it interacts with the baroclinic westerlies. These changes include loss of the upper-level symmetric TC warm core, development of a thermal advection dipole, and asymmetric ascent fields and eventual appearance of two regions of lower-tropospheric frontogenesis. These changes are described in the mean by Sinclair (2002) for the southwest Pacific basin and are the expected result of a vortex moving into and interacting with a baroclinic flow field (e.g., Doswell 1984). While some TCs progressively weaken as they advance into middle latitudes, others undergo a

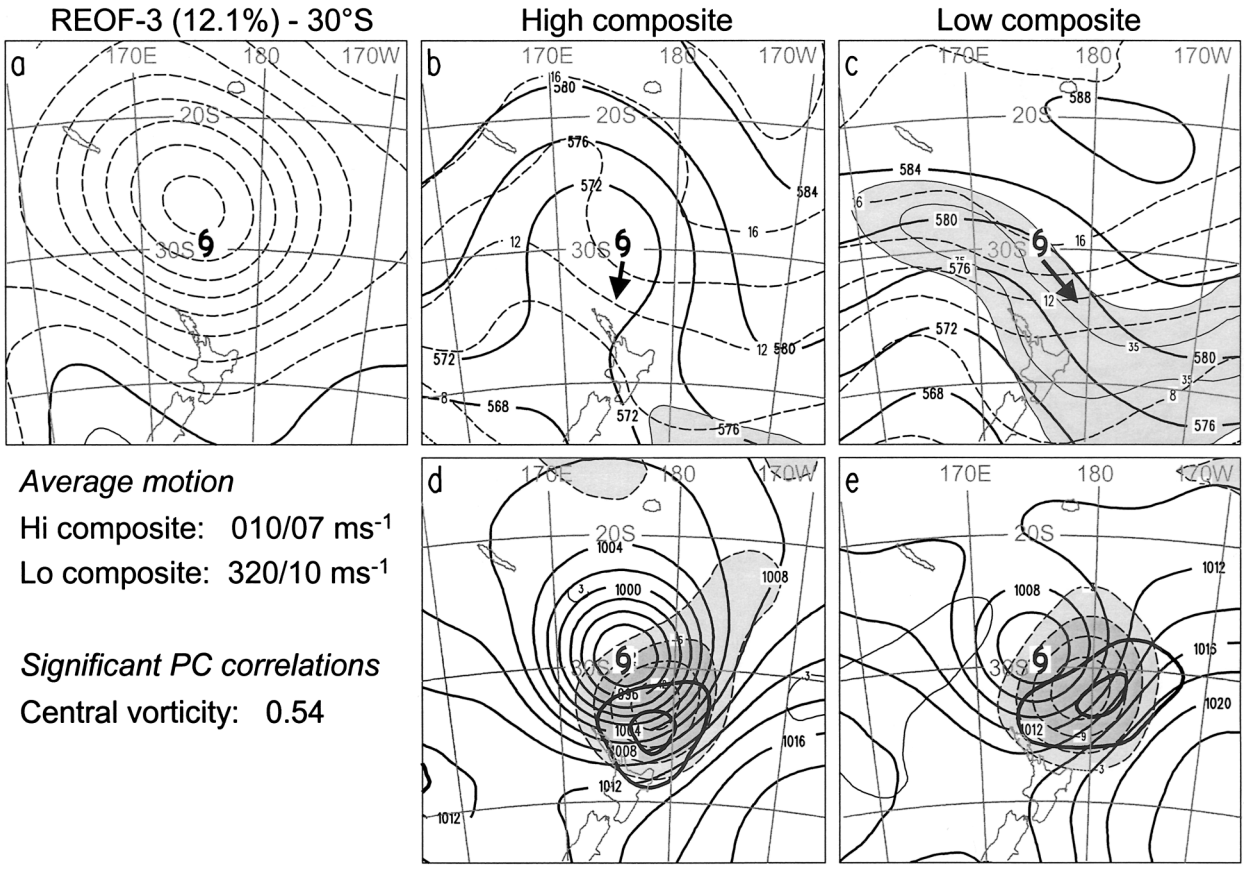

FIG. 11. As in Fig. 3 except for third rotated EOF eigenvector pattern.

period of extratropical regeneration, which typically occurs after a period of weakening as the decaying TC moves into middle latitudes.

Around 80% of the storms included in this study underwent one or more transient periods of restrengthening of central cyclonic vorticity by at least 2×10^{-5} s^{-1} following peak intensity in the Tropics. In section 5b, we examine characteristic synoptic signatures that accompany these redevelopment episodes. Almost all these cases of reintensification occurred near or poleward of 30°S, after the TC had acquired a baroclinic structure. Stronger reintensification, where there was a strengthening of central vorticity of more than 4×10^{-5} s^{-1} that lasted at least 24 h, occurred in 35% of cases. Analysis quality and data coverage clearly limit the accuracy of these statistics for storm reintensification. Furthermore, the assessment of whether or not a TC remnant has undergone regeneration is often subjective and varies depending on how reintensification is defined. Hart and Evans (2001) defined reintensification as when a cyclone deepens beyond to its pretransition intensity. Such a pressure-based definition is inappropriate for the SH because large central pressure falls typically occur when a SH cyclone moves toward a lower background pressure, regardless of whether or not surface winds around the cyclone have increased (Sinclair 1997).

Klein et al. (2000) noted that the potential for reintensification was dependent on the details of the midlatitude circulation and the geometry of the interaction. Sinclair (1993a) showed that the impetus for intensity change comes from interaction with migratory midlatitude disturbances in the westerlies. These interactions can weaken or strengthen the TC remnants, depending on the geometry of the interaction, the nature of the midlatitude trough, and the properties of the TC remnant.

In this section, we first identify the important dynamical and thermodynamic factors that modulate intensity change for southwest Pacific TCs entering middle latitudes. Then, episodes of midlatitude regeneration are singled out from the time series of central vorticity from each storm. Characteristic synoptic signatures that accompany regeneration are first identified, again by means of EOF analysis. Finally, a smaller set of more vigorous regeneration episodes is used to identify the upper-air signatures leading to more significant regeneration.

a. Dynamic and thermodynamic factors that modulate storm intensity

In this section, we identify factors that are most strongly correlated with variations in storm intensity as

TCs move into middle latitudes. The goal is to diagnose which factors most strongly modulate surface intensity changes. A set of thermodynamic and dynamic quantities is obtained for each track point and each quantity regressed against the set of central vorticity and pressure tendencies at each track point. The quantities used are obtained from Petterssen–Sutcliffe development theory (Petterssen 1956) as extended by Zwack and Okossi (1986). Similar diagnostics have been applied by Lupo et al. (1992), Rausch and Smith (1996), and Parsons and Smith (2004) to relate surface development to dynamic and thermodynamic forcings at various levels for cases of cyclone development near North America. Our approach follows Rausch and Smith (1996) except here we reformulate in storm-following coordinates in order to separate the advective effects associated with the translation of the storm system from the processes that force storm intensification. This is also required for consistency with the method used to compute central pressure and vorticity tendency following the moving TC as tracked.

As proposed by Johnson and Downey (1975) and applied by Sinclair and Elsberry (1986) and Sinclair and Cong (1992), the governing equation for the property of interest is expressed in the quasi-Lagrangian (QL) framework moving with velocity **C**, by replacing the Eulerian local rate of change, $\partial/\partial t$ by $\delta/\delta t - \mathbf{C}\cdot\boldsymbol{\nabla}$, where $\delta/\delta t$ is the change following the storm. Here, translation velocities, **C** were obtained as centered differences from the TC track coordinates. Storm-relative winds, $\mathbf{V} - \mathbf{C}$, are used in thermal and vorticity advection terms. Sinclair and Revell (2000) found that the storm-relative form of upper-level CVA, $-(\mathbf{V} - \mathbf{C})\cdot\boldsymbol{\nabla}\zeta$, was markedly better correlated with central pressure tendency than the usual Eulerian form, for 40 cases of SH cyclogenesis.

From the hydrostatic equation and the thermodynamic equation in QL coordinates, a relation for the thickness tendency following the storm can be obtained as

$$\frac{\delta}{\delta t}(\Phi_p - \Phi_b) = R\underbrace{\int_p^{p_b} [-(\mathbf{V} - \mathbf{C})\cdot\boldsymbol{\nabla}T]\, d\ \ln p}_{\text{TADV}} + R\underbrace{\int_p^{p_b} S\omega\, d\ \ln p}_{\text{ADIA}} + R\underbrace{\int_p^{p_b} \frac{\dot{Q}}{c_p}\, d\ \ln p}_{\text{LATH}}, \tag{2}$$

where Φ_b is the geopotential at pressure p_b near the bottom of the atmosphere (here 1000 hPa), Φ_p is that at pressure p, $S = -T\partial\ \ln\theta/\partial p$ is a static stability parameter, and $\dot{Q}/c_p$ is the diabatic heating rate. Diabatic heating (LATH) is assumed to arise from release of latent heat of condensation during resolvable saturated ascent and is computed following Sinclair (1993b). Precipitation is parameterized to commence for relative humidity above 60% to compensate for the averaging and nonrepresentativeness inherent in coarse-resolution gridpoint data.

To obtain an approximate expression for the geopotential tendency at pressure p, $\delta\Phi_p/\delta t$, we replace $\delta\zeta_p/\delta t$ in the vorticity equation by its geostrophic equivalent, $\delta/\delta t(\nabla^2\Phi_p/f)$ and take the inverse Laplacian, ∇^{-2}, of both sides and multiply by f to obtain

$$\frac{\delta\Phi_p}{\delta t} \approx \underbrace{\nabla^{-2}[-f(\mathbf{V} - \mathbf{C})\cdot\boldsymbol{\nabla}(\zeta + f)]}_{\text{VADV}} + \underbrace{\nabla^{-2}[-f(\zeta + f)\boldsymbol{\nabla}\cdot\mathbf{V}]}_{\text{VDIV}}, \tag{3}$$

where the smaller vertical advection and twisting terms have been neglected. In a similar formulation, Parsons and Smith (2004) found these to be an order of magnitude smaller than other vorticity equation terms. The ''inverse Laplacian,'' ∇^{-2}, is obtained as follows. The value, ψ, of $\nabla^{-2}\chi$ for some term χ, is obtained by solving $\nabla^2\psi = \chi$ using the method of sequential overrelaxation (Haltiner and Williams 1980, p. 159) with zero boundary conditions. Although this is strictly a double-space integral, we here use the ∇^{-2} symbology, since, mathematically, this is the inverse of the Laplacian operator. Substituting (3) into (2) and rearranging, we obtain

$$\underbrace{\frac{\delta\Phi_{1000}}{\delta t}}_{\Delta H} \approx \underbrace{-R\int_p^{1000} [-(\mathbf{V} - \mathbf{C})\cdot\boldsymbol{\nabla}T]\, d\ \ln p}_{-\text{TADV}} - \underbrace{R\int_p^{1000} S\omega\, d\ \ln p}_{-\text{ADIA}} - \underbrace{R\int_p^{1000} \frac{\dot{Q}}{c_p}\, d\ \ln p}_{-\text{LATH}} + \underbrace{\nabla^{-2}[-f(\mathbf{V} - \mathbf{C})\cdot\boldsymbol{\nabla}(\zeta + f)]_p}_{\text{VADV}} + \underbrace{\nabla^{-2}[-f(\zeta + f)\boldsymbol{\nabla}\cdot\mathbf{V}]_p}_{\text{VDIV}}. \tag{4}$$

This shows that 1000-hPa height falls (rises) occur in conjunction with net column-averaged warm (cold) advection, sinking (rising) motion, diabatic heating (cooling), plus cyclonic (anticyclonic) vorticity advection and divergence (convergence) at the top of the column. Friction and surface fluxes of heat and moisture are not included. Lupo et al. (1992) and Rausch and Smith (1996) found the direct contribution from surface exchanges to be small compared with other terms in (3), even for cyclones over the Gulf Stream or over land. Formulating (3) in terms of height rather than vorticity tendency avoids the necessity of applying a Laplacian to the thermodynamics terms in (2), reducing noise. Vertical integrals were obtained using cubic splines while

TABLE 4. Correlation of various terms with $\delta\Phi_{1000}/\delta t$. Here, VSUM is the sum of VADV + VDIV and NPTS is the number of track points in each latitude band used to compute the correlation coefficients. Only correlation coefficients significantly different from zero at the 95% level are shown.

Lat	∇THK	TADV	ADIA	LATH	VADV	VDIV	VSUM	NPTS
15°S	—	—	0.28	−0.30	0.26	—	0.29	193
20°S	—	−0.22	0.33	−0.31	0.29	−0.24	0.15	247
25°S	−0.30	—	—	—	0.28	−0.19	0.24	138
30°S	−0.23	—	0.34	−0.27	0.38	−0.18	0.41	106
35°S	−0.24	—	0.20	—	0.28	—	0.41	100
40°S	—	—	0.53	−0.47	0.49	—	0.63	62
45°S	−0.47	—	0.56	−0.54	0.71	−0.48	0.74	30

tendency terms were obtained as centered time differences, accurate to $O(\Delta t^2)$ [as compared with $O(\Delta t)$ for forward or backward differencing]. Forcing terms on the rhs of (4) were averaged in time using a 1–2–1 filter. These calculations were performed for all track points (except the first and last) for all 50 TCs. Correlations between the 1000-hPa height tendency, ΔH, and the other variables on the rhs of (4) were determined in six latitude bands and displayed in Table 4.

Results show that falling 1000-hPa heights (and surface pressures) are correlated with adiabatic cooling (ascent), latent heating, and upper-level cyclonic vorticity advection and divergence, as expected, with correlations increasing as the storms acquire extratropical characteristics south of 30°S. The term most strongly correlated with fluctuations in storm 1000-hPa heights, is upper-level QL vorticity advection. A more detailed analysis of the relation between surface pressure change and upper-level vorticity advection for various levels of the atmosphere revealed that the strongest correlations are always found at the jet level. North of 20°S, correlations are strongest at 200 hPa, at 250 hPa for 25° and 30°S, and at 300 hPa poleward of 35°S. Table 4 shows these terms for just 300 hPa. However, the sum of the two vorticity terms (VSUM) modulates surface pressure changes even more than CVA alone. This sum (of the advection of vorticity by the storm-relative flow and the divergence term) represents the net accumulation of absolute vorticity above the moving storm. From this simple correlation analysis, it is concluded that net import of cyclonic vorticity at the jet level above the storm is the synoptic-scale process having the most impact on surface development. This import of cyclonic vorticity occurs with the approach of an upper trough.

b. Synoptic signature of reintensifying cyclones

In the second part of this section, we use EOF analysis to identify characteristic synoptic signatures that accompany reintensification. A TC remnant is deemed to be reintensifying if the central 850-hPa vorticity falls (i.e., became more cyclonic) by more than 2×10^{-5} s^{-1} over a 24-h period following a period of weakening. Only intensification in the region poleward of 25°S was considered. The central vorticity change criterion was a trade-off between identifying events that were strongly reintensifying on the one hand and achieving a large enough count for statistical analysis on the other. Some storms decayed monotonically upon entering middle latitudes so were not candidates for regeneration. However, others had one or more transient or sustained periods of redevelopment south of 25°S, so were counted as previously. Forty-three episodes of modest extratropical redevelopment were found in this way. Rotated EOF analysis was performed on the 500-hPa fields accompanying these reintensification events in order to identify preferred synoptic signatures.

Figure 12 shows the spatial eigenvector pattern and the associated high and low composites for the first rotated EOF, which explains 61% of the case-to-case variability. In order to obtain enough cases for meaningful averaging, the high- and low-composite fields were obtained by averaging cases having PC amplitude more than 0.7 standard deviations above and below the temporal mean (rather than 1 standard deviation as before), resulting in nine included in the high composites and seven in the low composites. The principal mode of case-to-case variation involves fluctuations in 500-hPa height southwest of the center (Fig. 12a). High composites (Figs. 12b,d) feature a closed 500-hPa circulation and marked low-tropospheric baroclinity, particularly southeast of the storm, where considerable frontogenesis is occurring. The composite thermal gradient north and west of the low is weak. The surface low is moving due south beneath the equatorward entrance region of an upper jet and there is a surface high to the south.

The low composite (Figs. 12c,e) features the surface low moving more rapidly southeast beneath the poleward exit region of a stronger upper jet. Thermal and frontogenesis fields show two regions of frontogenesis (Fig. 12e)—one east of the center within strong warm advection and the other west and northwest of the center within cold advection (Fig. 12c). These suggest a structure similar to that of the Norwegian cyclone model, with distinct cold and warm fronts separated by a narrow warm sector.

Because the PC associated with the eigenvector pattern in Fig. 12 is highly correlated with latitude ($r = 0.72$), this variability is related to how far into the middle latitudes the TC has advanced. The nine intensifi-

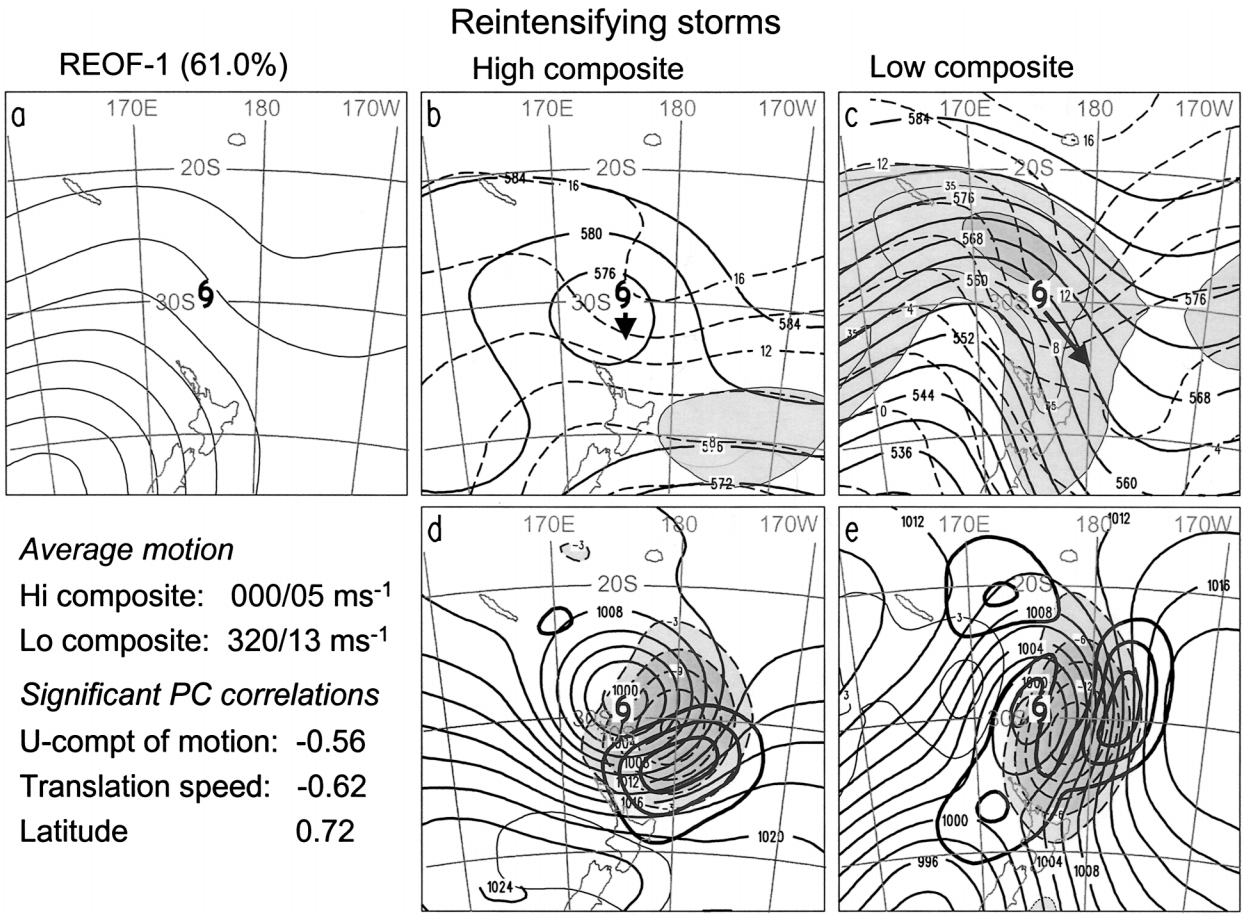

FIG. 12. As in Fig. 3 except for first rotated EOF eigenvector pattern for reintensifying storms. See text for more information.

cation episodes included in the high composites were all found between 25° and 33°S while the seven low-composite contributors were between 32° and 48°S. The PC was also correlated with motion ($r = -0.62$), with storms comprising the high composites having an average motion of 5 m s^{-1} toward the south while the low composites that had advanced deeper into the baroclinic westerlies moved southeast at 13 m s^{-1}. The higher-latitude low composites also featured larger intensification rates as measured by central vorticity tendency.

Both high and low composites in Fig. 12 exhibit favorable coupling with the upper jet, suggesting this to be a key factor for reintensification. This is consistent with the previous correlation analysis, which showed that TC intensity changes were closely related to net import and export of vorticity at the jet stream level. The lower-latitude low composites (Figs. 12b,d) are coupled with the equatorward entrance region of the upper jet and feature strong warm fronts and weak cold fronts. Reintensifying TCs further south move more rapidly southeast beneath the poleward exit region of a strong upper jet and exhibit both cold and warm fronts (Figs. 12c,e). Sometimes, the upstream jet in Fig. 12c originates as a separate migratory feature. For example, regeneration of Cyclone Patsy was triggered by a jet that propagated in from the west (Sinclair 1993a). Sinclair (2002) showed that of the cases that featured an upstream jet, about half involved a separate jet migrating from the west while the other half involved an in situ development in response to frontogenesis northwest of the center.

c. Rapid regeneration cases

Here, the set of the five most vigorous extratropical regeneration episodes is examined to identify the variety of synoptic signatures that accompany rapid reintensification and to determine the associated physical processes. These rapidly intensifying cases each have increases in cyclonic vorticity larger than 5×10^{-5} s^{-1} in 24 h.

Composites of terms in (4) for these five cases were first constructed (Fig. 13). A dipole of column-integrated warm (cold) advection is located east (west) of the surface center (Fig. 13a). Adiabatic cooling (Fig. 13b) is offset by diabatic heating. The sum of the three thermodynamic terms (not shown) features a weak dipole of column-integrated tropospheric warming east of

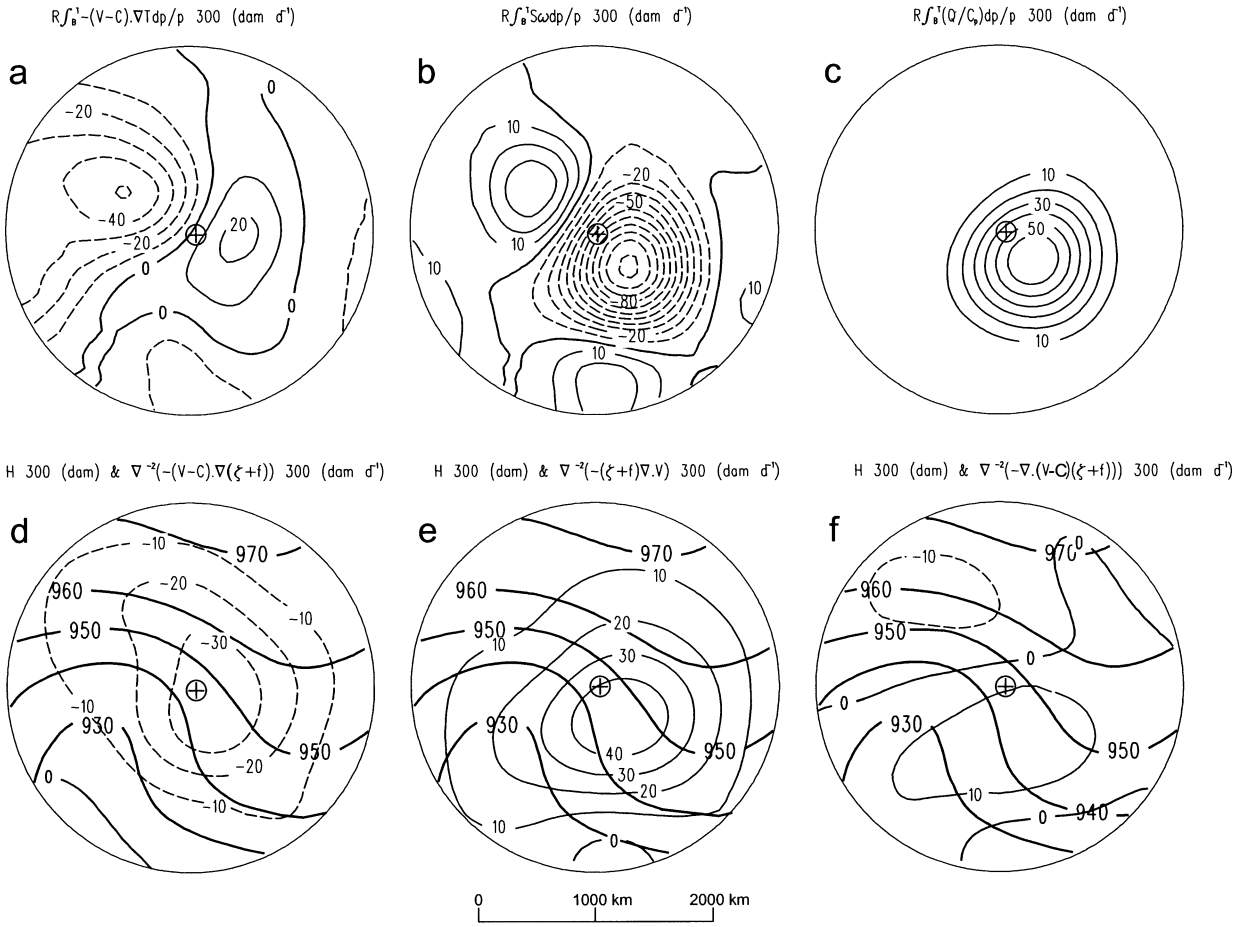

FIG. 13. Composite plots of terms from Eq. (4) (units ≡ dam day^{-1}) over a circular domain of radius 15° lat for strongly reintensifying storms, with positive values (thin solid), negative (dashed), and the zero contour (thicker solid). (a) TADV, (b) ADIA, (c) LATH, (d) VADV, (e) VDIV, and (f) the sum of VADV+VDIV. (a)–(c) For thermodynamic equation terms positive values contribute to thickness increases (warming), but to 1000-hPa height *falls.* For vorticity terms positive (negative) values contribute to 1000-hPa height rises (falls). (d)–(f) The 300-hPa height (solid, every 10 dam). The surface center is marked with a ⊕. See text for more details.

the composite low and cooling west of it. The 300-hPa vorticity terms (Figs. 13d–f) show CVA east of the trough almost offset by the divergence term. However, the sum of the vorticity terms, $\nabla^{-2}\{-\mathbf{\nabla}[(\mathbf{V} - \mathbf{C}) \cdot (\zeta + f)]\}$, representing 1000-hPa height changes from net accumulation of 300-hPa vorticity above the moving storm, shows a dipole of height falls in the trough and rises a little upstream from the ridge, consistent with the thermal terms. These height changes have the effect of amplifying the upper wave and decreasing its wavelength, which increases the CVA and divergence aloft. Composites constructed from the larger sample of 43 redevelopment episodes used for the EOF analysis in Fig. 12 yielded qualitatively similar results to Fig. 13 except the magnitude of terms was around half that in Fig. 13.

Individual charts at 250 hPa for these five cases for the period leading up to and including each redevelopment episode are shown in Fig. 14. These rapid cyclogenesis events occurred between 27° and 39°S, at an average latitude of 33°S. At the time of maximum cyclogenesis (bottom row), each storm lay beneath the superposition of the poleward exit region of an upstream jet and the equatorward entrance region of a downstream jet. Uccellini and Kocin (1987) find this to be a region of enhanced upper-level divergence and favored signature for rapid cyclogenesis. This double upper-jet signature is most strongly evident for Cyclone Bernie, which also featured the strongest redevelopment rate in the entire sample of 50 storms. Bernie's central vorticity became more cyclonic, changing from -8.8 to -14.7×10^{-5} s^{-1} over the 24-h period shown in Fig. 14. Details of the upper-jet evolution differ for each case. For Cyclones Sina and Bernie, the storm crosses from the warm side to the cold side of the strengthening upstream jet. For Cyclones Paul and Monica, the surface cyclone is more or less located beneath the equatorward entrance region of the downstream jet, with the upstream jet only evident at the time of maximum redevelopment. Cyclone Bola is located beneath the double signature

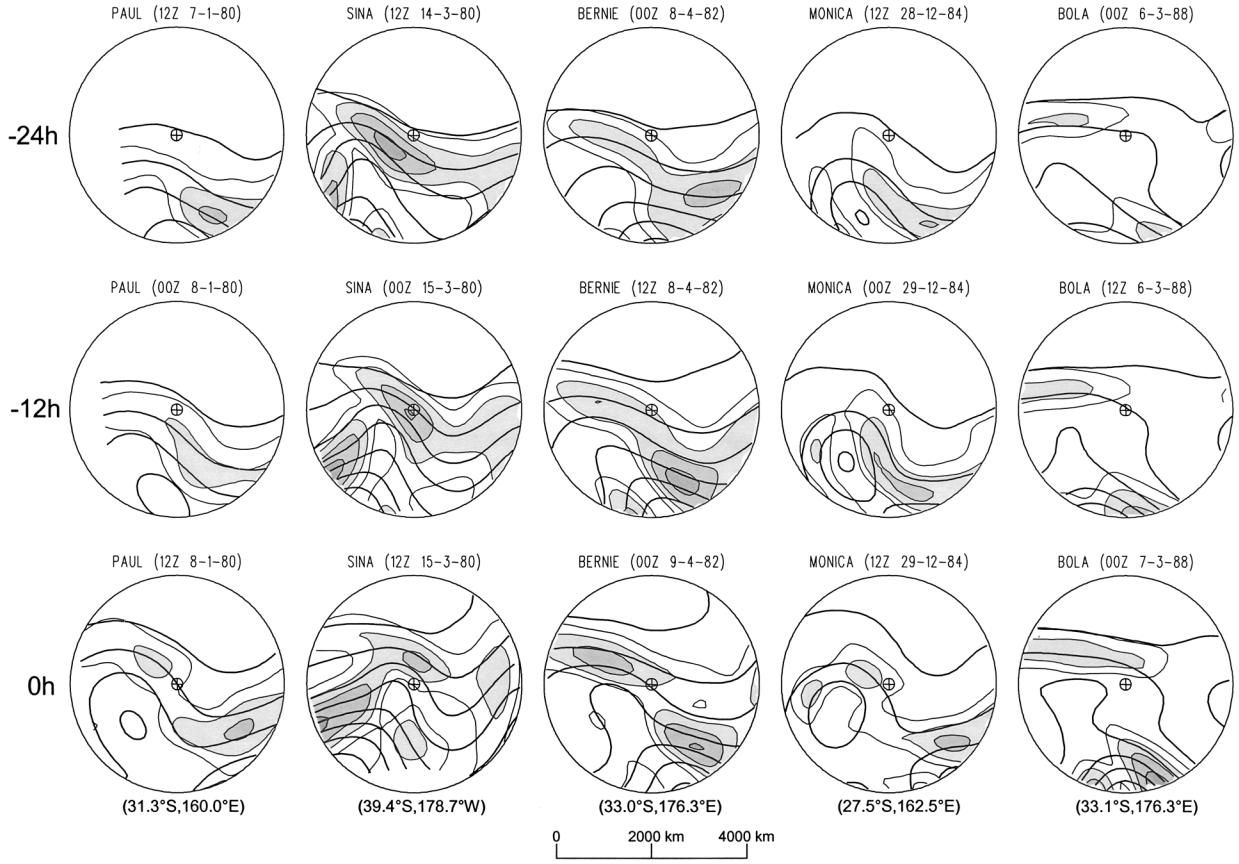

FIG. 14. Plots of 250-hPa height (solid, every 15 dam) and isotachs (every 10 m s^{-1} from 30 m s^{-1}, values >40 and 50 m s^{-1} shaded) over a circular domain of radius 20° lat for (top row) 24 h and (middle row) 12 h before max intensification, and (bottom row) at the time of max intensification for the five most rapidly redeveloping storms. The surface center is marked with a ⊕. See text for more detail.

throughout the period, with both jets slowly strengthening. Cyclogenesis occurs as the storm and the upstream jet migrate closer to the downstream jet. Each case also features an increase in upper-wave amplitude, consistent with the composite height changes in Fig. 13f.

d. Weakening cases

As a counterpoint, cases featuring a weakening surface circulation were also selected for composite analysis. A total of 30 times where central vorticity became less cyclonic at a rate exceeding 3×10^{-5} s^{-1} per day were found. As in Fig. 13, terms in (4) are composited (Fig. 15). At first sight, results are similar to those for the developing cases in Fig. 13 except terms are considerably smaller in magnitude. Thermodynamic terms again feature a thermal advection dipole, adiabatic ascent offset by diabatic heating, while vorticity terms are CVA offset by the divergence term. Here, however, the upper trough is more directly over the decaying storms. This results in CVA east of the surface center rather than directly above it as in Fig. 13. However, the fundamental difference lies in the sum of the two 300-hPa vorticity terms, which yield a net height increase in the trough. This results in flattening of the upper wave, reducing CVA and divergence.

6. Summary and conclusions

This second of two papers on extratropical transition in the southwest Pacific Ocean basin has identified characteristic midlatitude circulation types for 50 cases of extratropical transition near 30°S by means of EOF analysis. The first EOF, explaining nearly half of the storm-to-storm variance, represents variations in the strength of the westerlies in which the TC is embedded. As would be expected, this PC is highly correlated with the *u* component of storm translation. Tracks for the nine TCs where the PC was >1 standard deviation above the mean are mostly meridional whereas the seven low-composite cases featured more rapid zonal motion. The high composite is similar to the ''cradled'' classification of Foley and Hanstrum (1994), where the TC is cradled in a surface high to the southeast while the low composite features a vigorous 500-hPa trough to the south, with the TC moving rapidly southeast, like their ''capture'' cases. The low composites had just completed a

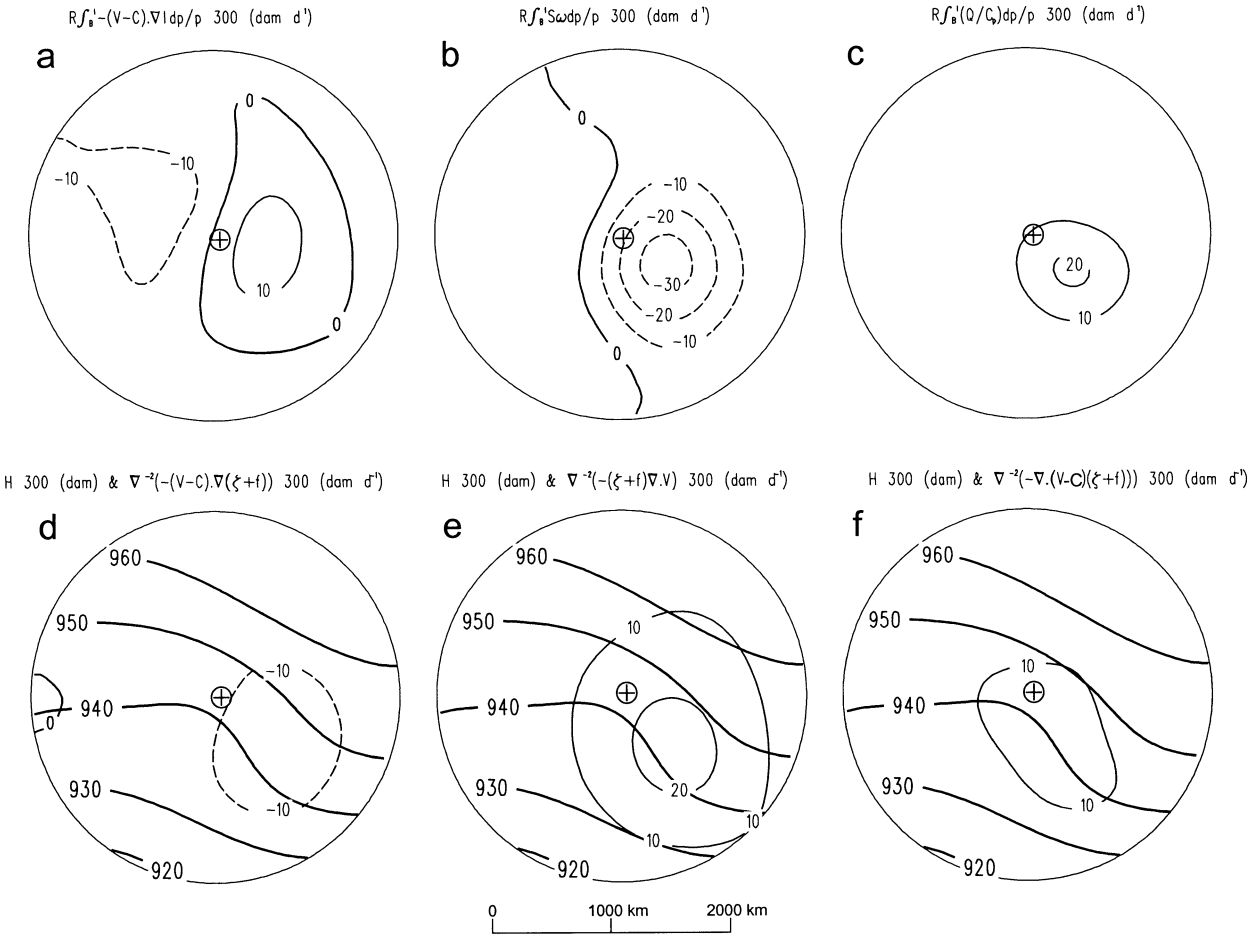

FIG. 15. As in Fig. 13 except for rapidly weakening storms.

period of intensification prior to reaching 30°S, and featured stronger upper jets and vertical wind shear.

The second rotated EOF reflects out-of-phase 500-hPa height variations southwest and southeast of the storm. Cyclones embedded in a circulation featuring a dominant trough to the southeast are located beneath the equatorward entrance region of an upper jet and undergo considerable reintensification because of stronger upper-level CVA and a stronger downstream ridge. Where the dominant trough was to the southwest, the main impact was to steer the TC poleward without intensification. The third rotated EOF, explaining a similar amount of variant to REOF-2, expressed variations in storm intensity.

It is interesting that both REOF-1 and REOF-3 were significantly correlated with the environment (REOF-1 through steering and REOF-3 through intensity) while REOF-2 is uncorrelated. It is possible that REOF-2 is related to the strength of the interaction between the storm and its environment. Evidence for this is found in the fact that the positively tilted high composites of REOF-2 developed after crossing 30°S while the negative composites weakened. Development for the high composites appeared to be related to a more favorable environment for upper-level divergence near the equatorward entrance region of an upper jet. The configuration was similar to the favorable distant interaction described by Hanley et al. (2001), where an upper trough approaches to within 1000 km of the TC remnant. Development occurs under the equatorward entrance region of the upper jet in such a way that the TC and the upper jet mutually reinforce each other.

A climatology of ET onset was also performed, using the objective diagnostic of Evans and Hart (2003). This showed that ET onset occurred at an average latitude 23°–25°S, with minimal seasonal variation. In comparison, NH TCs commence ET at an average latitude of 35°–45°N, with a marked seasonal variation. At the time of ET onset, the TCs were already absorbed into an upper-level midlatitude trough and were approaching the equatorward flank of a midlatitude low-level baroclinic zone.

Finally, factors responsible for extratropical regeneration were explored. Several studies (e.g., Palmén 1958; DiMego and Bosart 1982a,b; Bosart and Dean 1991; Sinclair 1993a) have shown that the approach of

an upper-level midlatitude trough from the west is necessary for reintensification as an extratropical cyclone. Regeneration of TC remnants has been likened to a Petterssen Type B cyclogenesis, where development occurs when CVA ahead of a strong upper-level trough moves over a region of low-level warm advection (Petterssen and Smebye 1971). Factors that modulate surface intensity poleward of 25°S were identified for the 50 storms. Of several diagnostic quantities, CVA at the jet level was the quantity most strongly correlated with surface development, confirming a role for jet-level CVA. Characteristic synoptic signatures for 43 episodes of extratropical reintensification revealed that reintensification occurred when the surface cyclone was located beneath the equatorward entrance region of an upper jet for storms between 28° and 34°S, and beneath the poleward exit region for storms farther south. The storms exhibiting particularly strong redevelopment each featured a strong double upper-jet signature formed by the combination of the upstream jet exit region and the downstream jet entrance region directly above the storm at the time of strongest intensification. Uccellini and Kocin (1987) found this to be a favorable region for rapid extratropical cyclogenesis. Sinclair (1993b) and Hanley (1999) found a similar double-jet signature aloft above the storm at the time of reintensification of a TC as an extratropical cyclone. Here, the composites for redeveloping storms revealed that strongest storm-relative upper-level CVA was directly above the surface low, with net vorticity fluxes resulting in rising heights in the upper ridge and falling heights in the trough. For weakening storms, CVA was east of the storm, with the net vorticity changes weakening the upper trough.

This study has shown that net import of cyclonic vorticity at the jet level is the primary factor controlling intensity variation of SH TCs undergoing ET. Presumably, this is because low inertial stability in the hurricane outflow layer renders the upper troposphere susceptible to changes in divergence above the surface low in response to the approach of an upper disturbance. However, as Hanley et al. (2001) point out, differences between approaching disturbances that lead to TC intensification and those that do not are often rather subtle, accounting for the difficulty experienced forecasting TC intensity change as a midlatitude trough approaches. This difficulty is compounded in the SH by a lack of observations. As Hanley et al. (2001) observe, there are some situations where the upper jet appears to be forcing development and others where the upper jets appear to be the result of the TC–trough interaction. Clearly, more observations and improved analyses near the jet stream level might improve forecasts of ET. However, numerical models probably offer the best means of determining cause and effect during ET.

Acknowledgments. The southwest Pacific tropical cyclone database was kindly provided to NIWA by MetService (formerly New Zealand Meteorological Service) while gridded atmospheric analyses were provided by NCEP. The author is grateful to three anonymous reviewers who provided comments that improved the manuscript. This research was funded by the New Zealand Foundation for Research, Science and Technology under Contract CO1831.

REFERENCES

Bosart, L. F., and D. B. Dean, 1991: The Agnes rainstorm of June 1972: Surface feature evolution culminating in inland storm redevelopment. *Wea. Forecasting,* **6,** 515–537.

——, and G. M. Lackmann, 1995: Postlandfall tropical cyclone reintensification in a weakly baroclinic environment: A case study of Hurricane David (September 1979). *Mon. Wea. Rev.,* **123,** 3268–3291.

Brand, S., and C. P. Guard, 1978: Extratropical storm evolution from tropical cyclones in the western North Pacific Ocean. Naval Environmental Prediction Tech. Rep. TR 78-02, 20 pp.

Browning, K. A., G. Vaughan, and P. Panagi, 1998: Analysis of an extratropical cyclone after its reintensification as a warm core extratropical cyclone. *Quart. J. Roy. Meteor. Soc.,* **124,** 2329–2356.

——, A. J. Thorpe, A. Mantani, D. Parsons, M. Griffiths, P. Panagi, and E. M. Dicks, 2000: Interactions of tropopause depressions with an ex–tropical cyclone and sensitivity of forecasts to analysis errors. *Mon. Wea. Rev.,* **128,** 2734–2755.

Carr, F. H., and L. F. Bosart, 1978: A diagnostic evaluation of rainfall predictability for Tropical Storm Agnes, June 1972. *Mon. Wea. Rev.,* **106,** 363–374.

Christenson, W. F., and R. A. Bryson, 1966: An investigation of the potential of component analysis for weather classification. *Mon. Wea. Rev.,* **94,** 697–709.

Craddock, J. M., and C. R. Flood, 1969: Eigenvectors for representing the 500-mb geopotential surface over the Northern Hemisphere. *Quart. J. Roy. Meteor. Soc.,* **95,** 576–593.

Davies, H. C., C. Schär, and H. Wernli, 1991: The palette of fronts and cyclones within a baroclinic wave development. *J. Atmos. Sci.,* **48,** 1666–1688.

DiMego, G. J., and L. F. Bosart, 1982a: The transformation of Tropical Storm Agnes into an extratropical cyclone. Part I: The observed fields and vertical motion computations. *Mon. Wea. Rev.,* **110,** 385–411.

——, and ——, 1982b: The transformation of Tropical Storm Agnes into an extratropical cyclone. Part II: Moisture, vorticity and kinetic energy budgets. *Mon. Wea. Rev.,* **110,** 412–433.

Doswell, C. A., III, 1984: A kinematic analysis of frontogenesis associated with a nondivergent vortex. *J. Atmos. Sci.,* **41,** 1242–1248.

Evans, J. L., and R. E. Hart, 2003: Objective indicators of the life cycle evolution of extratropical transition for Atlantic tropical cyclones. *Mon. Wea. Rev.,* **131,** 909–925.

Foley, G. R., and B. N. Hanstrum, 1994: The capture of tropical cyclones by cold fronts off the west coast of Australia. *Wea. Forecasting,* **9,** 577–592.

Haltiner, G. J., and R. T. Williams, 1980: *Numerical Prediction and Dynamic Meteorology.* John Wiley and Sons, 477 pp.

Hanley, D. E., 1999: The effect of trough interactions on tropical cyclone intensity change. Ph.D. thesis, The University at Albany, State University of New York, 164 pp.

——, J. Molinari, and D. Keyser, 2001: A composite study of the interactions between tropical cyclones and upper-tropospheric troughs. *Mon. Wea. Rev.,* **129,** 2570–2584.

Harr, P. A., and R. L. Elsberry, 2000: Extratropical transition of tropical cyclones over the western North Pacific. Part I: Evolution of structural characteristics during the transition process. *Mon. Wea. Rev.,* **128,** 2613–2633.

——, ——, and T. F. Hogan, 2000: Extratropical transition of tropical

cyclones over the western North Pacific. Part II: The impact of midlatitude circulation characteristics. *Mon. Wea. Rev.,* **128,** 2634–2653.
Hart, R. E., and J. L. Evans, 2001: A climatology of the extratropical transition of Atlantic tropical cyclones. *J. Climate,* **14,** 546–564.
Hartmann, D. L., 1995: A PV view of zonal flow vacillation. *J. Atmos. Sci.,* **52,** 2561–2576.
Hill, H. W., 1970: The precipitation in New Zealand associated with the cyclone of early April 1968. *N. Z. J. Sci.,* **13,** 641–662.
Johnson, D. R., and W. K. Downey, 1975: Azimuthally averaged transport and budget equations for storms: Quasi-Lagrangian diagnostics. *Mon. Wea. Rev.,* **103,** 967–979.
Joliffe, I. T., 1986: *Principal Component Analysis.* Springer-Verlag, 271 pp.
Kalnay, E., and Coauthors, 1996: The NCEP/NCAR 40-Year Reanalysis Project. *Bull. Amer. Meteor. Soc.,* **77,** 437–471.
Karoly, D. J., 1990: The role of transient eddies in low-frequency zonal variations in the Southern Hemisphere circulation. *Tellus,* **42A,** 41–50.
Kidson, J. W., 1988: Indices of the Southern Hemisphere zonal wind. *J. Climate,* **1,** 183–194.
——, 1994: An automated procedure for the identification of synoptic types applied to the New Zealand region. *Int. J. Climatol.,* **14,** 711–721.
Klein, P. M., 1997: Extratropical transition of western North Pacific tropical cyclones. M.S. thesis, Department of Meteorology, Naval Postgraduate School, Monterey, CA, 101 pp. [NTIS ADA-341-420.]
——, P. A. Harr, and R. L. Elsberry, 2000: Extratropical transition of western North Pacific tropical cyclones: An overview and conceptual model of the transformation stage. *Wea. Forecasting,* **15,** 373–395.
Kutzbach, J. E., 1967: Empirical eigenvectors of sea-level pressure, surface temperature and precipitation complexes over North America. *J. Appl. Meteor.,* **6,** 791–802.
Lupo, A. R., P. J. Smith, and P. Zwack, 1992: A diagnosis of the explosive development of two extratropical cyclones. *Mon. Wea. Rev.,* **120,** 1490–1523.
McTaggart-Cowan, R., J. R. Gyakum, and M. K. Yau, 2001: Sensitivity testing of extratropical transitions using potential vorticity inversions to modify initial conditions: Hurricane Earl case study. *Mon. Wea. Rev.,* **129,** 1617–1636.
North, G. R., T. L. Bell, R. F. Cahalan, and F. J. Moeng, 1982: Sampling errors in the estimation of empirical orthogonal functions. *Mon. Wea. Rev.,* **110,** 699–706.
O'Lenic, E. A., and R. E. Livezey, 1988: Practical considerations in the use of rotated principle component analysis (RPCA) in diagnostic studies of upper air heights. *Mon. Wea. Rev.,* **116,** 1682–1689.
Palmén, E., 1958: Vertical circulation and release of kinetic energy during the development of Hurricane Hazel into an extratropical storm. *Tellus,* **10,** 1–21.
Parsons, K. E., and P. J. Smith, 2004: An investigation of extratropical cyclone development using a scale-separation technique. *Mon. Wea. Rev.,* **132,** 956–974.
Petterssen, S., 1936: Contribution to the theory of frontogenesis. *Geofys. Publ.,* **11** (6), 1–27.
——, 1956: *Weather Analysis and Forecasting.* 2d ed. Vol. 1. McGraw-Hill, 428 pp.
——, and S. J. Smebye, 1971: On the development of extratropical storms. *Quart. J. Roy. Meteor. Soc.,* **97,** 457–482.
Rausch, R. L. M., and P. J. Smith, 1996: A diagnosis of a model-simulated explosively developing extratropical cyclone. *Mon. Wea. Rev.,* **124,** 875–904.
Richman, M. B., 1981: Obliquely rotated principal components: An improved meteorological map typing technique. *J. Appl. Meteor.,* **20,** 1145–1159.
——, 1986: Rotation of principal components. *Int. J. Climatol.,* **6,** 293–335.
Ritchie, E. A., and R. L. Elsberry, 2003: Simulations of the extratropical transition of tropical cyclones: Contributions by the midlatitude upper-level trough to reintensification. *Mon. Wea. Rev.,* **131,** 2112–2128.
Schultz, D. M., D. Keyser, and L. F. Bosart, 1998: The effect of large-scale flow on low-level frontal structure and evolution in midlatitude cyclones. *Mon. Wea. Rev.,* **126,** 1767–1791.
Sinclair, M. R., 1993a: Synoptic-scale diagnosis of the extratropical transition of a southwest Pacific tropical cyclone. *Mon. Wea. Rev.,* **121,** 941–960.
——, 1993b: A diagnostic study of the extratropical precipitation resulting from Tropical Cyclone Bola. *Mon. Wea. Rev.,* **121,** 2690–2707.
——, 1997: Objective identification of cyclones and their circulation intensity, and climatology. *Wea. Forecasting,* **12,** 595–612.
——, 2002: Extratropical transition of southwest Pacific tropical cyclones. Part 1: Climatology and mean structure changes. *Mon. Wea. Rev.,* **130,** 590–609.
——, and R. L. Elsberry, 1986: A diagnostic study of baroclinic disturbances in polar air streams. *Mon. Wea. Rev.,* **114,** 1957–1983.
——, and X. Cong, 1992: Polar airstream cyclogenesis in the Australasian region: A composite study using ECMWF analyses. *Mon. Wea. Rev.,* **120,** 1950–1972.
——, and M. Revell, 2000: Classification and composite diagnosis of extratropical cyclogenesis events in the southwest Pacific. *Mon. Wea. Rev.,* **128,** 1089–1105.
Thorncroft, C. D., and S. C. Jones, 2000: The extratropical transitions of Hurricanes Felix and Iris in 1995. *Mon. Wea. Rev.,* **128,** 947–972.
——, B. J. Hoskins, and M. E. McIntyre, 1993: Two paradigms of baroclinic wave life-cycle behavior. *Quart. J. Roy. Meteor. Soc.,* **119,** 17–55.
Uccellini, L. W., and P. C. Kocin, 1987: The interaction of jet streak circulations during heavy snow events along the east coast of the United States. *Wea. Forecasting,* **2,** 289–308.
Zwack, P., and B. Okossi, 1986: A new method for solving the quasi-geostrophic omega equation by incorporating surface pressure tendency data. *Mon. Wea. Rev.,* **114,** 655–666.